Table 1. Blood Phe, *in vivo* Phe oxidation and liver vector DNA in female *Pah*^{enu2} mice after 8 weeks of scAAV8/LP1-mPAH injection

Genotype/dose (vg)	Phe (mg/dl)	$\Delta^{13}CO_2$ (‰)	Vector DNA (c/dg)
WT/none ($n = 7$)	0.7 ± 0.1	38.9 ± 14.8	ND
Pah^{enu2}/none ($n = 8$)	32.5 ± 6.2	1.1 ± 0.8	ND
Pah^{enu2}/1×10^{11} ($n = 4$)	1.8 ± 0.5	32.8 ± 13.4	1.5 ± 0.3
Pah^{enu2}/1×10^{12} ($n = 4$)	1.0 ± 0.3	39.5 ± 13.0	27.3 ± 16.0

ND, not determined.

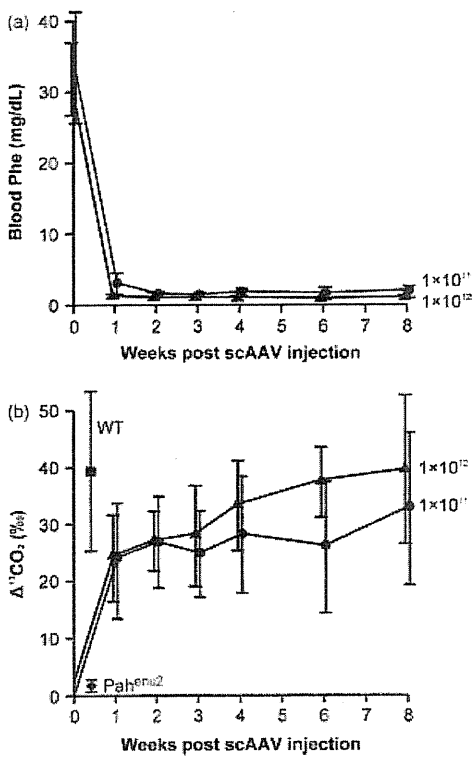

Figure 3. Short-term efficacy of scAAV8/LP1-mPAH in female *Pah*^{enu2} mice after i.p. injection. (a) Weekly blood Phe (mg/dl) levels are depicted as the mean ± SD. (b) *In vivo* Phe oxidation ($\Delta^{13}CO_2$‰) levels are represented as the mean ± SD of each dosage group. Circles, BTBR-*Pah*^{enu2} given 1×10^{11} vg of scAAV8 ($n = 4$); triangles, BTBR-*Pah*^{enu2} given 1×10^{12} vg ($n = 4$); square, wild-type BTBR (WT, $n = 7$); diamond, untreated BTBR-*Pah*^{enu2} (Pah^{enu2}, $n = 8$)

Following a single i.p. injection of scAAV8/LP1-mPAH, a dramatic decrease of blood Phe was observed in female *Pah*^{enu2} (Figure 3a). In mice receiving 1×10^{11} vg of vector, blood Phe was decreased from 33.3 ± 7.8 mg/dl to 3.0 ± 1.5 mg/dl ($n = 4$; $p < 0.01$) in 1 week and kept within the normal range 2–8 weeks post-injection (Table 1). In mice receiving 1×10^{12} vg of vector, hyperphenylalaninemia was corrected even more rapidly and uniformly; blood Phe was normalized in 1 week (from 31.7 ± 5.1 to 1.2 ± 0.3 mg/dl, $n = 4$; $p < 0.01$) through 8 weeks after treatment (Table 1). Between these two dosage groups, the blood Phe concentration was not significantly different, except for the data obtained 2 weeks post-i.p. ($p < 0.05$). With normalization of blood Phe, hypopigmentation in the treated mice was gradually ameliorated. Patchy black hair emerged by week 2, and the animals recovered the WT coat color by week 8.

In parallel with blood Phe analysis, we evaluated the *in vivo* oxidation capacity for Phe by a non-invasive breath test. In this assay, administered ^{13}C-Phe is converted to [1-^{13}C]Tyr by PAH, which is then broken down to yield homogentisic acid and $^{13}CO_2$ by two enzymatic reactions. Eventually, $^{13}CO_2$ is liberated into breath, and the $^{13}CO_2$ concentration (as a ratio to $^{12}CO_2$) is measured by infrared spectrophotometry or GC-MS. Because our initial experiments showed that GC-MS offered lower background, this method was used in the subsequent investigation. The amount of $^{13}CO_2$ production ($\Delta^{13}CO_2$) is determined by the difference between the $^{13}CO_2$ concentration of the breath samples collected before and after ^{13}C-Phe infusion. Because a significant fraction of input ^{13}C-Phe is metabolized through the above pathway where PAH catalyses the rate-limiting step, we can evaluate PAH activity by measuring $\Delta^{13}CO_2$ [27]. WT mice showed positive $\Delta^{13}CO_2$ values without an apparent gender difference (males: 45.5 ± 8.8‰, $n = 7$; females: 38.9 ± 14.8‰, $n = 7$). By contrast, untreated *Pah*^{enu2} mice produced very little, if any, $\Delta^{13}CO_2$ in the breath test (males: 1.0 ± 0.6‰, $n = 3$; females: 1.1 ± 0.8‰, $n = 8$), resulting from the absence of PAH activity (Table 1). The impaired *in vivo* Phe oxidation was rapidly corrected following scAAV8/LP1-mPAH injection, in a reciprocal fashion to blood Phe reduction (Figure 3b). In the female *Pah*^{enu2} mice receiving 1×10^{11} vg of vector, $\Delta^{13}CO_2$ was improved from 0.9 ± 0.8‰ to 23.6 ± 10.2‰ in 1 week ($n = 4$; $P < 0.05$) and maintained in a near-normal to normal range thereafter. In mice receiving 1×10^{12} vg of vector, $\Delta^{13}CO_2$ was increased from 1.4 ± 0.9‰ to 24.2 ± 7.5‰ at week 1 ($n = 4$; $p < 0.01$) with an upward tendency until week 8 (Table 1).

After 8 weeks post-i.p., the animals were euthanized for tissue DNA analysis for vector biodistribution. The vector content in the liver was 1.5 ± 0.3 and 27.3 ± 16.0 copies/diploid genome (c/dg) in the low- (1×10^{11} vg, $n = 4$) and high-dosage (1×10^{12} vg, $n = 4$) groups, respectively ($p < 0.05$; Table 1). Although the vector DNA was barely detected (<0.01 c/dg) in the spleen and gonads from mice given 1×10^{12} vg of vector, a trace amount of vector (0.3–0.5 c/dg) was present in these viscera from the mice receiving 1×10^{12} vg. The DNA analysis recapitulated a very strong liver tropism of scAAV8 vectors as reported previously [21].

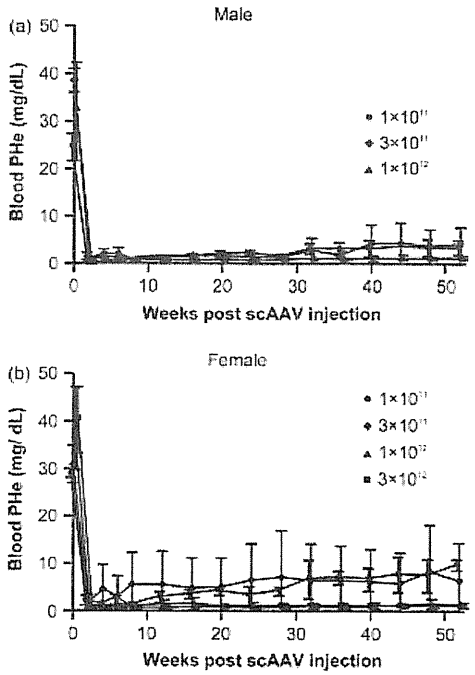

Figure 4. Long-term efficacy of i.p.-injected scAAV8/LP1-mPAH in *Pah*^{enu2} mice. (a) Male *Pah*^{enu2} mice were administered either 1×10^{11} vg (circles, $n = 4$), 3×10^{11} vg (diamonds, $n = 3$) or 1×10^{12} vg (triangles, $n = 3$) of scAAV8/LP1-mPAH, and the data are depicted as the mean ± SD blood Phe (mg/dl) versus weeks post-injection of scAAV8. (b) Female *Pah*^{enu2} mice were given either 1×10^{11} vg (circles, $n = 3$), 3×10^{11} vg (diamonds, $n = 3$), 1×10^{12} vg (triangles, $n = 4$) or 3×10^{12} vg (squares, $n = 4$) of scAAV8/LP1-mPAH, and the data are shown as the mean ± SD blood Phe (mg/dl)

Long-term correction of hyperphenylalaninemia in both genders

Encouraged by the shot-term efficacy of scAAV8/LP1-mPAH vector in female *Pah*^{enu2}, we treated several cohorts of PKU mice with the same vector for longer observation ($n = 3$–4 each). Male and female *Pah*^{enu2} mice (6–8 weeks of age) were given either 1×10^{11}, 3×10^{11} or 1×10^{12} vg of scAAV8/LP1-mPAH by i.p. injection. An additional female cohort was given a higher dose (3×10^{12} vg), in consideration of the possibility of temporary transgene expression in this gender. The treated mice were phlebotomized for blood Phe analysis every 2–4 weeks, and Figure 4 shows the kinetics of blood Phe concentration for 1 year following vector administration. In males, Phe levels decreased to normal with all doses (1×10^{11} vg, from 25.1 ± 2.3 to 1.1 ± 0.3 mg/dl; 3×10^{11} vg, from 38.3 ± 2.7 to 0.8 ± 0.6 mg/dl; 1×10^{12} vg, from 32.5 ± 9.7 to 0.4 ± 0.1 mg/dl) at week 2 (Figure 4a). All males with 1×10^{12} vg ($n = 3$) and two out of three males with 3×10^{11} vg maintained normal blood Phe (<1.7 mg/dl) throughout 1-year observation, whereas one with 3×10^{11} vg showed a mild elevation (8–9 mg/dl) from 32 weeks post-i.p. One male with 1×10^{11} vg upheld normal blood Phe, whereas three out of four in this cohort had slightly increased blood Phe from 32 weeks that was within the therapeutic range (2–6 mg/dl). A similar, although slightly limited long-term efficacy was observed in females (Figure 4b). In the female *Pah*^{enu2} mice with 3×10^{12} vg ($n = 4$) or 1×10^{12} vg ($n = 4$) of vector, blood Phe decreased to normal in 2 weeks (from 40.2 ± 7.0 to 0.7 ± 0.4 mg/dl, and 38.5 ± 8.7 to 0.6 ± 0.2 mg/dl, respectively) and maintained that level for 1 year. In females with 3×10^{11} vg, two out of three animals sustained normal blood Phe, whereas the other mouse lost control after 4 weeks with moderate hyperphenylalaninemia (10–15 mg/dl). In females with 1×10^{11} vg ($n = 3$), blood Phe was corrected initially (from 29.1 ± 1.0 to 1.5 ± 0.5 mg/dl at week 4), although the level was gradually increased to near-normal (2–6 mg/dl at weeks 12–28) and then mild hyperphenylalaninemic range (6–10 mg/dl at weeks 32–52). Despite such variability being observed in a limited number of animals, the reduction of blood Phe was significant in all the cohorts throughout the observation period. This result clearly demonstrated the superb efficacy of scAAV8/LP1-mPAH vector in treating murine PKU. We assumed that the vector threshold dose

Table 2. Remote phase blood Phe, *in vivo* Phe oxidation and vector DNA in the liver

Gender	Dose (vg)	Phe (mg/dl)	$\Delta^{13}CO_2$ (‰)	Vector DNA (c/dg)
Male	1×10^{11}	3.9	18.31	0.88
	1×10^{11}	3.0	32.54	0.57
	3×10^{11}	1.7	52.18	1.34
	3×10^{11}	2.1	19.54	1.16
	1×10^{12}	3.3	45.34	9.95
	1×10^{12}	1.2	ND	7.85
Female	1×10^{11}	12.4	3.96	0.17
	1×10^{11}	8.9	1.57	0.22
	3×10^{11}	4.2	5.62	0.48
	1×10^{12}	1.6	60.44	3.13
	3×10^{12}	1.3	23.31	6.38
	3×10^{12}	2.4	62.95	6.47
	3×10^{12}	1.2	55.60	9.26

ND, not determined.

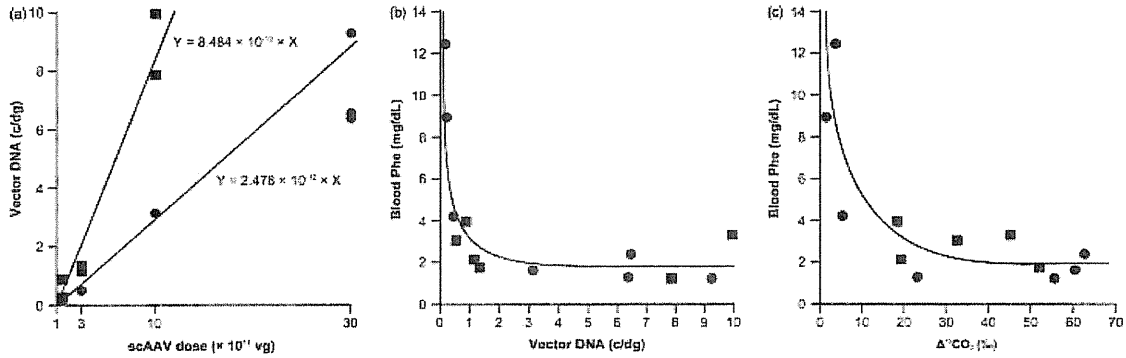

Figure 5. Relationships among vector dose, blood Phe, *in vivo* Phe oxidation and vector DNA content in remote phase. (a) Relationship between the given dose of scAAV8/LP1-mPAH (vg; *x*-axis) and vector DNA content in the liver (c/dg; *y*-axis). Plots with males (squares) fit a regression line of $y = 8.484 \times 10^{-12}x$, whereas plots with females (circles) fit a line of $y = 2.478 \times 10^{-12}x$. (b) Relationship between the vector DNA in the liver (c/dg; *x*-axis) and blood Phe (mg/dl; *y*-axis). Males (squares) and females (circles) fit a single hyperbolic-like curve. (c) Relationship between *in vivo* Phe oxidation ($\Delta^{13}CO_2$‰; *x*-axis) and blood Phe (mg/dl; *y*-axis). Plots of males (squares) and females (circles) fit a single hyperbolic-like curve

to correct hyperphenylalaninemia was 1×10^{11} vg or less for male Pah^{enu2} mice, and slightly over 1×10^{11} vg for females that would be a half-log higher. A gender-specific difference appears to exist with scAAV8 as well, although the barrier in female animals may be smaller than that with ssAAV vectors.

Correlation between transduction rate and function in remote phase

After confirming the long-term efficacy of the scAAV8 vector in both genders, we examined *in vivo* Phe oxidation and tissue DNA in several Pah^{enu2} mice later than 1 year after scAAV8 injection. Table 2 summarizes the data obtained for six males and seven females evaluated at 60–80 weeks post-i.p., and Figure 5 shows the relationships among the parameters chosen. The amount of vector DNA in the liver showed a linear relationship with the given vector dose, and was not saturated within the dose range used in the present study (Figure 5a). Compared with the data for 8 weeks post-i.p. (Table 1), the vector DNA content in the treated females was approximately one-tenth in the remote phase, suggesting a slow but substantial vector loss. The lines best fit the data were $y = 8.484 \times 10^{-12}x$ ($r^2 = 0.962, p < 0.0001$) for males and $y = 2.478 \times 10^{-12}x$ ($r^2 = 0.967, p < 0.0001$) for females, respectively (x, vector dose in vg; y, vector DNA in the liver in c/dg). Thus, male livers were more efficiently transduced than female livers by 3.4-fold, in agreement with the above assumption of vector doses for correcting hyperphenylalaninemia in these genders.

Once the liver was transduced, the vector appeared to impact on Phe metabolism in the same, or nearly identical mode in both genders. Figure 5b shows the relationship between liver vector copy number and blood Phe. Plots for male (squares) and female (circles) livers appear to fit into quite analogous, if not identical, hyperbolic-like curves. Blood Phe levels were steeply reduced to normal as the vector copy number increased from 0 to 1 c/dg, and no further reduction was observed with more vector DNA in the liver. Therefore, Phe was normalized by the presence of 1 or more vector c/dg, regardless of gender. The result suggests that the larger dose requirement of scAAV8 to correct female hyperphenylalaninemia resulted not from poorer transgene expression but from a lower transduction efficiency. Figure 5c shows the relationship between *in vivo* Phe oxidation and blood Phe. Again, plots of both males (squares) and females (circles) appear to fit an almost identical hyperbolic-like curve. Earlier preclinical studies showed that recovery of 10–20% of normal PAH activity was sufficient to normalize blood Phe in Pah^{enu2} mice, in agreement with accumulated clinical data [1,9,31]. Because we observed a significant baseline deviation and fluctuation of $\Delta^{13}CO_2$ in WT animals (Table 1) partly because of the relative BH_4 insufficiency *in vivo* [27], it was difficult to calculate the actual recovery of Phe oxidation capacity of the treated Pah^{enu2} mice. Nevertheless, it is noteworthy that some animals showed physiological or even higher levels of Phe catabolism, even for extended periods (60–80 weeks) after scAAV8 injection.

Discussion

In the present study, we showed a long-term efficacy of a scAAV8 vector for murine PKU in both genders. To our knowledge, the vector allowed the longest duration (up to 80 weeks) of correcting hyperphenylalaninemia, particularly in female Pah^{enu2}, by gene transfer. We previously showed successful correction of hyperphenylalaninemia in Pah^{enu2} mice with a ssAAV5 vector, although the effect was partial and transient in females [7]. Type 8-pseudotyping of that vector increased the initial efficacy by more than ten-fold, although the therapeutic benefit waned over time in female Pah^{enu2}. Other studies also recognized a similar female disadvantage with ssAAV8, although it was

milder than that with ssAAV2 and ssAAV5 [14,32]. On the other hand, Ding *et al.* [10] normalized blood Phe in both male and female *Pah*^{enu2} mice with a ssAAV8 vector up to 42 weeks. Following an injection of relatively large dose (5×10^{12} vg) of ssAAV8, they found very high copy number (>1000 c/dg) of vector DNA in the liver of their animals, which was 20–50-fold greater than than that in other studies including our own. If this was indeed the case, such an excess amount of vector, at least in part, may account for the adequate PAH expression that would overcome the female disadvantage.

In our experimental setting, the scAAV genome structure finally allowed a robust and stable liver transduction in female mice. In accordance with our results, recent studies have demonstrated the advantage of scAAV vectors in liver-directed gene transfer, particularly in combination with the serotype 8 capsid [32–35]. Pañeda *et al.* [32] extensively studied the efficiency of pseudotyped ssAAV and scAAV vectors and showed a significant advantage of scAAV8 in female mice. Furthermore, using the same vector platform (scAAV8/LP1) as in the present study, Vaessen *et al.* [33] showed a near-physiological transgene expression in a murine apolipoprotein A-I deficiency model, whereas Wu *et al.* [34] suggested that further fine-tuning of the vector should increase the efficacy. Because the therapeutic end point for PKU gene transfer is relatively high (>10% of normal PAH activity), these investigations are quite encouraging. Interestingly, Nathwani *et al.* [35] observed that preadministration of bortezomib, a proteasome inhibitor, augmented liver transduction with a scAAV8 vector in female mice by two-fold, whereas the enhancement in male animals was more modest. A detailed understanding of the molecular events in AAV transduction should allow such pharmacological support for better gene transfer in actual clinical settings.

One of the issues addressed in the present study was how many AAV vector copies in the liver would be required for persistent phenotypic correction of PKU. In the analysis at 8 weeks post-i.p., we found 1.5 ± 0.3 c/dg following 1×10^{11} vg i.p. and 27.3 ± 16.0 c/dg following 1×10^{12} vg i.p. (Table 1), whereas other studies detected more AAV genomes in their mouse liver. For example, Harding *et al.* [9] detected 16–51 c/dg of vector DNA in the mouse liver 8–17 weeks after they injected 5×10^{11} vg of ssAAV8, and Nakai *et al.* [36] found 58.2 ± 10.9 c/dg of vector 6 weeks after 3×10^{11} vg of ssAAV8. Presumably, our method of AAV administration (i.p.) was relatively less efficient compared to the PV injection that these investigators carried out. However, the reason for the large discrepancy compared to another study [10] (>1000 c/dg) is unknown. After initial transduction of the liver, the recombinant AAV genomes may be gradually degraded or diluted because they are present as episomes [37]. Indeed, we observed that the vector DNA was decreased to one-tenth in the animal liver after 1 year. At this stage, we demonstrated that the threshold of the therapeutic vector DNA in the tissue was approximately 1 c/dg. To extend gene transfer efficacy, a new strategy may be required. Integrating vectors are maintained if they do not elicit immunological responses, although most of them have some genotoxicity at the expense of stability through mitosis. Site-specific integrases may offer safer and stable transduction [38], although the delivery vehicle for such a strategy is currently underdeveloped. Alternatively, targeting extrahepatic tissues for PKU gene therapy has been discussed. In particular, skeletal muscle is an attractive target because of its slow turnover and easy accessibility [3,39,40]. One of the problems with this approach is how to deliver cofactor BH_4 to the exogenously expressed PAH in a clinically feasible way.

In summary, a single injection of scAAV8 vector corrected hyperphenylalaninemia in male and female PKU mice for the longest period reported to date. Although it is difficult to translate murine experiments into human PKU directly, the accumulating safety and efficacy studies of AAV gene transfer to larger animals are very informative. Together with an encouraging result obtained in a haemophilia B clinical trial started recently [41], these investigations will help to develop a safe and long-lasting gene transfer strategy for PKU treatment.

Acknowledgements

The authors are grateful to Takashi Matsushita and Miyoko Mitsu for vector preparation, as well as Kiyomi Aoki for the manuscript artwork. This work was supported in part by Grants-in-Aid for Scientific Research from the Ministry of Education, Culture, Sports, Science and Technology-Japan (#20591230). The authors have no relevant conflicts of interest to declare.

References

1. Scriver CR, Kaufman S. Hyperphenylalaninemia: phenylalanine hydroxylase deficiency. In The Metabolic and Molecular Bases of Inherited Disease, Scriver CR, Beaudet AL, Sly WS, Valle D (eds). McGraw-Hill: New York, NY, 2001; 1667–1724.
2. Eisensmith RC, Woo SLC. Gene therapy for phenylketonuria. *Eur J Pediatr* 1996; **155**: S16–S19.
3. Thöny B. Long-term correction of murine phenylketonuria by viral gene transfer: liver versus muscle. *J Inherit Metab Dis* 2010; **33**: 677–680.
4. Shedlovsky A, McDonald JD, Symula D, Dove WF. Mouse models of human phenylketonuria. *Genetics* 1993; **134**: 1205–1210.
5. McDonald JD, Charlton CK. Characterization of mutations at the mouse phenylalanine hydroxylase locus. *Genomics* 1997; **39**: 402–405.
6. Laipis PJ, Charron C, Ross K, *et al.* Long-term correction of phenylketonuria in an animal model by recombinant AAV-based gene therapy. *J Inherit Metab Dis* 2002; **25**: 615–616.
7. Mochizuki S, Mizukami H, Ogura T, *et al.* Long-term correction of hyperphenylalaninemia by AAV-mediated gene transfer leads to behavioral recovery in phenylketonuria mice. *Gene Ther* 2004; **11**: 1081–1086.
8. Oh H, Park E, Kang S, Jo I, Jung S. Long-term enzymatic and phenotypic correction in the phenylketonuria

mouse model by adeno-associated virus vector-mediated gene transfer. *Pediatr Res* 2004; **56:** 278–284.
9. Harding CO, Gillingham MB, Hamman K, *et al.* Complete correction of hyperphenylalaninemia following liver-directed, recombinant AAV2/8 vector-mediated gene therapy in murine phenylketonuria. *Gene Ther* 2006; **13:** 457–462.
10. Ding Z, Georgiev P, Thöny B. Administration-route and gender-independent long-term therapeutic correction of phenylketonuria (PKU) in a mouse model by recombinant adeno-associated virus 8 pseudotyped vector-mediated gene transfer. *Gene Ther* 2006; **13:** 587–593.
11. Davidoff AM, Ng CYC, Zhou J, Spence Y, Nathwani AC. Sex significantly influences transduction of murine liver by recombinant adeno-associated viral vectors through an androgen-dependent pathway. *Blood* 2003; **102:** 480–488.
12. Gao GP, Alvira MR, Wang L, Calcedo R, Johnston J, Wilson JM. Novel adeno-associated viruses from rhesus monkeys as vectors for human gene therapy. *Proc Natl Acad Sci USA* 2002; **99:** 11854–11859.
13. Davidoff AM, Gray JT, Ng CYC, *et al.* Comparison of the ability of adeno-associated viral vectors pseudotyped with serotype 2, 5 and 8 capsid proteins to mediate efficient transduction of the liver in murine and nonhuman primate models. *Mol Ther* 2005; **11:** 875–888.
14. Wang L, Calcedo R, Nichols TC, *et al.* Sustained correction of disease in naive and AAV2-pretreated hemophilia B dogs: AAV2/8-mediated, liver-directed gene therapy. *Blood* 2005; **105:** 3079–3086.
15. Russell DW, Kay MA. Adeno-associated virus vectors and hematology. *Blood* 1999; **94:** 864–874.
16. Nakai H, Storm TA, Kay MA. Recruitment of single-stranded recombinant adeno-associated virus vector genomes and intermolecular recombination are responsible for stable transduction of liver in vivo. *J Virol* 2000; **74:** 9451–9463.
17. McCarty DM, Monahan PE, Samulski RJ. Self-complementary recombinant adeno-associated virus (scAAV) vectors promote efficient transduction independently of DNA synthesis. *Gene Ther* 2001; **8:** 1248–1254.
18. McCarty DM, Fu H, Monahan PE, Toulson CE, Naik P, Samulski RJ. Adeno-associated virus terminal repeat (TR) mutant generates self-complementary vectors to overcome the rate-limiting step to transduction in vivo. *Gene Ther* 2003; **10:** 2112–2118.
19. Wang Z, Ma H-I, Li J, Sun L, Zhang J, Xiao X. Rapid and highly efficient transduction by double-stranded adeno-associated virus vectors in vitro and in vivo. *Gene Ther* 2003; **10:** 2105–2111.
20. Niwa H, Yamamura K, Miyazaki J. Efficient selection for high-expression transfectants with a novel eukaryotic vector. *Gene* 1991; **108:** 193–200.
21. Nathwani AC, Gray JT, Ng CYC, *et al.* Self-complementary adeno-associated virus vectors containing a novel liver-specific human factor IX expression cassette enable highly efficient transduction of murine and nonhuman primate liver. *Blood* 2006; **107:** 2653–2661.
22. Matsushita T, Elliger S, Elliger C, *et al.* Adeno-associated virus vectors can be efficiently produced without helper virus. *Gene Ther* 1998; **5:** 938–945.
23. Okada T, Nomoto T, Shimazaki K, *et al.* Adeno-associated virus vectors for gene transfer to the brain. *Methods* 2002; **28:** 237–247.
24. Okada T, Nomoto T, Yoshioka T, *et al.* Large-scale production of recombinant viruses by use of a large culture vessel with active gassing. *Hum Gene Ther* 2005; **16:** 1212–1218.
25. Ishiwata A, Mimuro J, Mizukami H, *et al.* Liver-restricted expression of the canine factor VIII gene facilitates prevention of inhibitor formation in factor VIII-deficient mice. *J Gene Med* 2009; **11:** 1020–1029.
26. Lock M, McGorray S, Auricchio A, *et al.* Characterization of a recombinant adeno-associated virus type 2 reference standard material. *Hum Gene Ther* 2010; **21:** 1273–1285.
27. Kure S, Sato K, Fujii K, *et al.* Wild-type phenylalanine hydroxylase activity is enhanced by tetrahydrobiopterin supplementation in vivo: an implication for therapeutic basis of tetrahydrobiopterin-responsive phenylalanine hydroxylase deficiency. *Mol Genet Metab* 2004; **83:** 150–156.
28. Mochizuki S, Mizukami H, Kume A, *et al.* Adeno-associated virus (AAV) vector-mediated liver- and muscle-directed transgene expression using various kinds of promoters and serotypes. *Gene Ther Mol Biol* 2004; **8:** 9–18.
29. Ogura T, Mizukami H, Zhang YY, *et al.* Tissue distribution of expression using AAV8-based vectors after intramuscular injection and other routes of delivery. *Mol Ther* 2005; **11:** S334.
30. Ogura T, Mizukami H, Mimuro J, *et al.* Utility of intraperitoneal administration as a route of AAV serotype 5 vector-mediated neonatal gene transfer. *J Gene Med* 2006; **8:** 990–997.
31. Fang B, Eisensmith RC, Li XHC, *et al.* Gene therapy for phenylketonuria: phenotypic correction in a genetically deficient mouse model by adenovirus-mediated hepatic gene transfer. *Gene Ther* 1994; **1:** 247–254.
32. Pañeda A, Vanrell L, Mauleon I, *et al.* Effect of adeno-associated virus serotype and genomic structure on liver transduction and biodistribution in mice of both genders. *Hum Gene Ther* 2009; **20:** 908–917.
33. Vaessen SFC, Veldman RJ, Comijn EM, *et al.* AAV gene therapy as a means to increase apolipoprotein (Apo) A-I and high-density lipoprotein-cholesterol levels: correction of murine ApoA-I deficiency. *J Gene Med* 2009; **11:** 697–707.
34. Wu Z, Sun J, Zhang T, *et al.* Optimization of self-complementary AAV vectors for liver-directed expression results in sustained correction of hemophilia B at low vector dose. *Mol Ther* 2008; **16:** 280–289.
35. Nathwani AC, Cochrane M, McIntosh J, *et al.* Enhancing transduction of the liver by adeno-associated viral vectors. *Gene Ther* 2009; **16:** 60–69.
36. Nakai H, Fues S, Storm TA, Muramatsu S, Nara Y, Kay MA. Unrestricted hepatocyte transduction with adeno-associated virus serotype 8 vectors in mice. *J Virol* 2005; **79:** 214–224.
37. Nakai H, Yant SR, Storm TA, Fuess S, Meuse L, Kay MA. Extrachromosomal recombinant adeno-associated virus vector genomes are primarily responsible for stable liver transduction in vivo. *J Virol* 2001; **75:** 6969–6976.
38. Calos MP. The ΦC31 integrase system for gene therapy. *Curr Gene Ther* 2006; **6:** 633–645.
39. Ding Z, Harding CO, Rebuffat A, Elzaouk L, Wolff JA, Thöny B. Correction of murine PKU following AAV-mediated intramuscular expression of a complete phenylalanine hydroxylating system. *Mol Ther* 2008; **16:** 673–681.
40. Rebuffat A, Harding CO, Ding Z, Thöny B. Comparison of adeno-associated virus pseudotype 1, 2, and 8 vectors administered by intramuscular injection in the treatment of murine phenylketonuria. *Hum Gene Ther* 2010; **21:** 463–477.
41. Nathwani AC, Rosales C, McIntoh J, *et al.* Early clinical trial results following administration of a low dose of a novel self complementary adeno-associated viral vector encoding human factor ix in two subjects with severe haemophilia B. *Hum Gene Ther* 2010; **21:** 1362.

Cancer Science
The official journal of the Japanese Cancer Association JCA

Development of a mouse model for lymph node metastasis with endometrial cancer

Kayoko Takahashi,[1,2,4] Yasushi Saga,[2] Hiroaki Mizukami,[1,3] Yuji Takei,[2] Masashi Urabe,[1] Akihiro Kume,[1] Mitsuaki Suzuki[2] and Keiya Ozawa[1,3]

[1]Division of Genetic Therapeutics, Center for Molecular Medicine, Tochigi; [2]Department of Obstetrics and Gynecology, Jichi Medical University, Tochigi, Japan

(Received June 9, 2011/Revised September 5, 2011/Accepted September 5, 2011/Accepted manuscript online September 12, 2011/Article first published online October 17, 2011)

Controlling lymph node metastasis is currently a key issue in cancer therapy. Lymph node metastasis is one of the most important prognostic factors in various types of cancers, including endometrial cancer. Vascular endothelial growth factor-C (VEGF-C) plays a crucial role in lymphangiogenesis, and is implicated to play an important role in lymph node metastasis. To evaluate the role of VEGF-C in lymph node metastasis, we developed an animal model by using an endometrial cancer cell line, HEC1A. This cell line is not invasive by nature and secretes moderate amounts of VEGF-C; intrauterine injection of HEC1A cells into Balb/c nude mice resulted in uterine cancer with lymph node metastasis after 8 weeks. To analyze the contribution of VEGF-C to lymph node metastasis, its corresponding gene was stably introduced into HEC1A cells (HEC1A/VEGF-C), which then produced more than 10 times the amount of VEGF-C. The number of lymph node metastases was significantly higher in HEC1A/VEGF-C cells than in HEC1A cells (3.2 *vs* 1.1 nodes/animal, respectively). Augmented lymphangiogenesis was observed within tumors when HEC1A/VEGF-C cells were inoculated. These results indicate that VEGF-C plays a critical role in lymph node metastasis, in addition to serving as a platform to test the efficacy of various therapeutic modalities against lymph node metastasis. (*Cancer Sci* 2011; 102: 2272–2277)

Endometrial cancer is one of the most common gynecological malignancies, and the fourth most common malignancy.[1] The overall prognosis of endometrial cancer is considered to be better than that for other types of gynecological malignancies, because the disease can be detected in its early stages. However, the prognosis of patients with advanced stages of endometrial cancer is still poor, owing to the lack of effective treatment modalities. Furthermore, the overall survival rate for such patients has not improved over the past 30 years.[1] One of the most important prognostic factors in endometrial cancer is lymph node metastasis.[2,3] Therefore, it is vital to develop new treatment modalities that focus on lymph node metastasis.

The factors involved in lymphangiogenesis and lymph node metastasis were recently elucidated; it has become clear that vascular endothelial growth factor (VEGF)-C is a significant contributor.[4–6] Vascular endothelial growth factor-C is a 38-kDa glycoprotein that acts through a tyrosine kinase-type receptor, VEGF receptor 3 (VEGFR3). It is suggested that during malignancy, VEGF-C produced by tumor and/or interstitial cells promotes lymph node metastasis.[7] Vascular endothelial growth factor-C expression in uterine endometrial carcinoma was found to be related to both lymphatic vessel invasion and lymph node metastasis in a study with 228 surgical cases of endometrial cancer.[4]

The development of an adequate animal model is critical for facilitating research on lymph node metastasis. Therefore, we aim to develop a suitable animal model by using endometrial cancer cells.

Materials and Methods

Cells and plasmids. Human endometrial cancer cell lines, HEC1A and HEC50B, were obtained from the Japanese Collection of Research Bioresources; the cell lines were authenticated through the multiplex PCR method, using short tandem repeats,[8] and were maintained as described previously.[9,10] The Ishikawa cell line (clone 3H12) was a gift from Dr. M. Nishida (Department of Obstetrics and Gynecology, National Hospital Organization, Kasumigaura Medical Center, Ibaraki, Japan), and was maintained as described previously.[11] The VEGF-C sequence was obtained by PCR, using the following primer set against human placental cDNA: forward, 5′-ATGCACTTTGCTGGGCTTCTT-3′; reverse, 5′-CAATCTTAGCTCATTTGTGGTCT-3′. The VEGF-C expression plasmid, pCMV–VEGF-C–internal ribosome entry site (IRES)–blasticidin S-resistance (*bsr*) gene, was constructed by inserting the VEGF-C sequence into the *Eco*RI and *Xba*I sites of pCMV–IRES–*bsr*.[12]

Development of stably-transduced cells. The VEGF-C expression plasmid, pCMV–VEGF-C–IRES–*bsr*, and the control, pCMV–luciferase (LUC)–IRES–*bsr*,[12] were introduced into HEC1A cells by using the standard calcium phosphate method. The structures of these plasmids are shown in Figure 1. According to our previous experiments, introducing pCMV–LUC–IRES–*bsr* does not alter the growth, migration, invasive capacity, anticancer drug sensitivity, or the radiosensitivity of cells.[13]

Cells were selected in the presence of 10 μg/mL blasticidin S hydrochloride (Funakoshi, Tokyo, Japan) for 2 weeks, and the resistant cells were collected as HEC1A/VEGF-C and HEC1A/LUC.

Vascular endothelial growth factor-C quantification in culture supernatant. The culture medium was replaced by fresh medium without serum. After 48 h of culturing, the supernatants of each cell line (HEC1A, HEC1A/LUC, HEC1A/VEGF-C, HEC50B, and Ishikawa 3H12) were collected and subjected to VEGF-C analysis, using a Quantikine human ELISA kit (R&D Systems, Minneapolis, MN, USA).

***In vitro* cell growth kinetics.** The HEC1A, HEC1A/VEGF-C, and HEC1A/LUC cells were dispersed so that 1×10^5 cells were present in each well of 3.5-cm plastic dishes. After culturing, the cells were dislodged using 0.05% trypsin–EDTA every 24 h to determine the number of cells by using a hemocytometer.

***In vivo* tumor growth by subcutaneous inoculation.** Five- to 6-week-old female Balb/c nude mice (CLEA Japan, Tokyo, Japan) were used for the tumor growth experiments. All animal experiments were conducted according to the institutional and national guidelines for animal experiments. The HEC1A,

[3]To whom correspondence should be addressed.
E-mail: miz@jichi.ac.jp; kozawa@jichi.ac.jp
[4]Present address: The Cancer Institute Hospital of the Japanese Foundation for Cancer Research, Tokyo, Japan.

doi: 10.1111/j.1349-7006.2011.02099.x

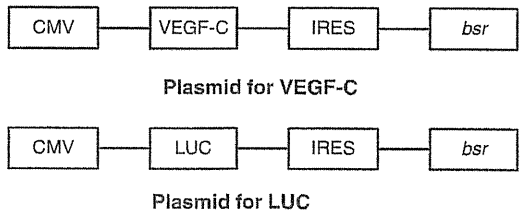

Fig. 1. Structure of the plasmids used in this study. Plasmids encoding vascular endothelial growth factor-C (VEGF-C) driven by the CMV promoter were used for cellular transduction. Plasmids encoding luciferase (LUC) were used as controls. *bsr*, blasticidin S-resistance gene; IRES, internal ribosome entry site.

HEC1A/VEGF-C, and HEC1A/LUC cells were implanted dorsally under the skins of the mice at 5×10^6 cells/site. Tumor volume was estimated using the formula: $0.5 \times L \times W^2$, where L and W indicate length and width in millimeters, respectively ($n = 5$).[14]

***In utero* transplantation of tumor cells.** Five- to 6- week-old female BALB/c nude mice (CLEA Japan) were used for the *in utero* experiments. A diagram of the injection procedure is shown in Figure 2. A laparotomy with a transverse incision was performed under general anesthesia, followed by ligation of the openings of the uterus at three locations, using 4-0 Vicryl (Ethicon, New Brunswick, NJ, USA). Tumor cells (5×10^6 cells) suspended in 50 μL PBS were injected into the uterine cavities by using a syringe with a 29-gauge needle. The left and right uterine cavities received similar volumes of cell suspension. The incisions were closed after the uterine tubes were inspected for proper enlargement and the absence of leakage. Uterine involvement and tumor development, especially lymph node metastasis, were evaluated periodically by laparotomy after the mice were killed.

Histological analysis of the animals. The animals were killed as scheduled, and all of the abdominal, thoracic, and retroperitoneal organs were inspected macroscopically. The metastatic lesions, uteri, and other organs showing possible signs of metastasis were microscopically evaluated for tumor progression. To estimate lymph node metastasis by size, recognizable lymph nodes were excised, and the presence of tumor metastasis was evaluated by histology in the first and second animal series. In the third and fourth animal series, the number of lymph node metastases was counted by enumerating lymph nodes larger than 3 mm in longitudinal diameter and evaluating them histologically.

Lymphangiogenesis in the subcutaneous tumor. At 2 weeks after the subcutaneous transplantation of corresponding cells (5×10^6 cells per animal) into the back, the mice ($n = 4$) were killed, and the subcutaneous tumors were excised. After fixation

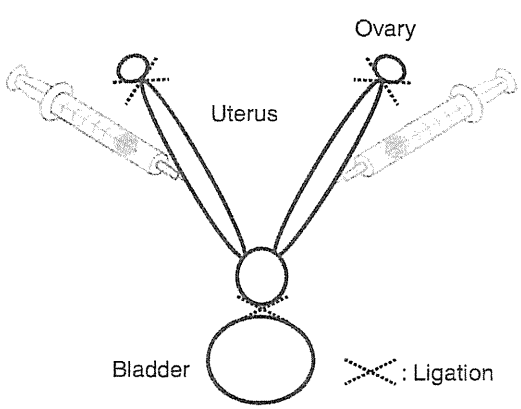

Fig. 2. Tumor cell injection procedure. After laparotomy under general anesthesia, all ends of the uterus were closed by ligation, ensuring the settlement of tumor cells within the uterine cavity. Following ligation, the cells were injected by puncturing the uterine wall. Abdominal incision was sutured after confirming that there was no leakage of cell suspension from the uterus.

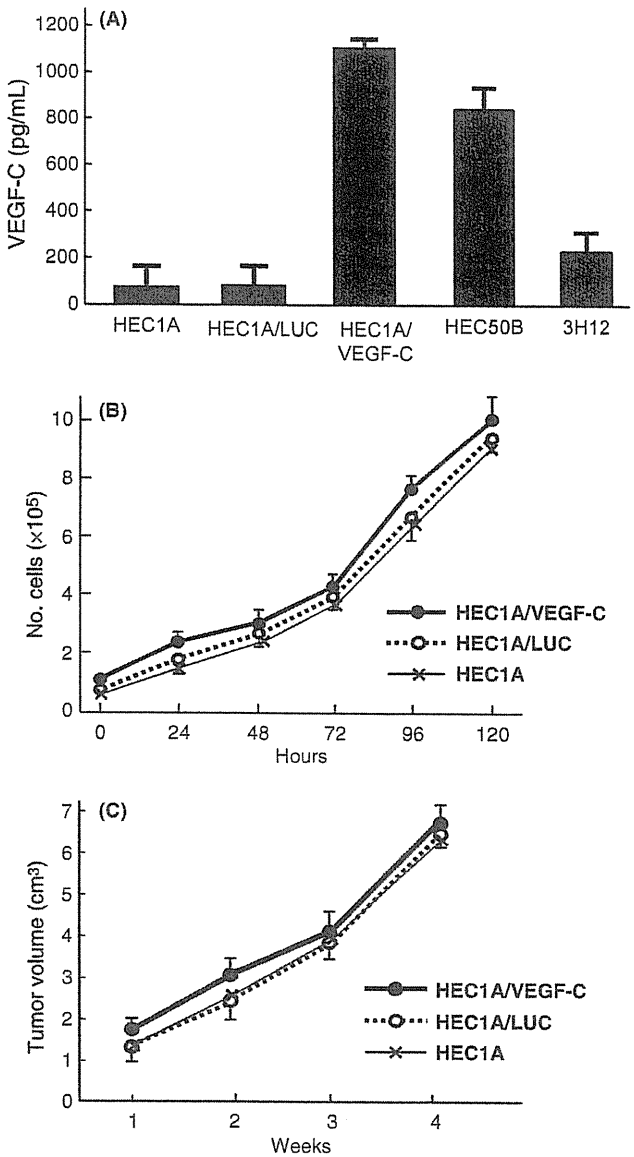

Fig. 3. (A) Vascular endothelial growth factor-C (VEGF-C)- or luciferase (LUC)-encoding plasmids were introduced into HEC1A cells by calcium phosphate transfection. Resultant cells were maintained, and the culture media were replaced with serum-free media upon confluence. After 48 h, the VEGF-C concentration of culture supernatants was determined by ELISA. Supernatant from the HEC1A/VEGF-C cells exhibited 10 times the concentration of VEGF-C, compared to the HEC1A or HEC1A/LUC cells. (B) Cells were dispersed at a concentration of 1×10^5/well in six well plates and were subsequently cultured. Cells were dislodged and counted after 24 h. There were no differences in the growth among these cell lines. (C) Growth of subcutaneous tumors after injection. Cells were subcutaneously injected into Balb/c nude mice (5×10^6 cells/site), and the tumor volumes were determined during follow up. No differences were found between these cells *in vivo*.

of the tumors in 4% paraformaldehyde, frozen sections were sliced, and antigen enhancement was done by heating the sections at 121°C in sodium citrate buffer (0.01 mol/L, pH 6.0) for 10 min, and endogenous peroxidase was blocked with 3% H_2O_2. The sections were incubated overnight at 4°C with a 1:500 dilution of anti-VEGFR3 antibody (Abcam, Cambridge, UK) as the primary antibody recognizing lymphatic endothelial cells, and then reacted with the secondary antibody, that is, the peroxidase-conjugated antirat antibody (Simple Stain Mouse MAX-PO, Rat; Nichirei, Tokyo, Japan) at room temperature for 30 min, followed by color development with diaminobenzidine. The number of newly-formed lymph vessels was counted under a light microscope at ×20 magnification. A single section was prepared per mouse in four animals per group, and new lymph vessels were counted in the four sections and averaged.

Verification. All *in vitro* experiments were performed at least three times.

Results

***In vitro* production of VEGF-C and cell growth kinetics.** Culture supernatants of the HEC1A and HEC1A/LUC cells showed similar VEGF-C concentrations, whereas the HEC1A/VEGF-C cells produced much greater concentrations of VEGF-C (Fig. 3A). There were no differences in the growth properties of the HEC1A/LUC and HEC1A/VEGF-C cells, both *in vitro* and *in vivo* (Fig. 3B,C).

***In vivo* transplantation of tumor cells.** When the HEC1A/LUC cells were injected into the uterus, subsequent tumor development was observed; therefore, follow ups were performed to determine the occurrence of lymph node metastases (Table 1). At 4 weeks, one of five mice developed metastasis; at 6 weeks, two of four developed metastasis. At 8 weeks after injection, all of the mice in the first series exhibited lymph node metastasis. Consequently, the second series was carried out using a larger number of animals, which again resulted in the successful development of metastases within the same time frame. At 8 weeks, the uterus was swollen and the endometrium was filled with tumor cells (Fig. 4A,B). Marked infiltrations into the enlarged lymph nodes were also noted in mice injected with the HEC1A/LUC (Fig. 4C) and HEC1A/VEGF-C (Fig. 4D,E) cells.

Relationship between lymph node size and metastasis. Upon analysis of the model mice, 40 lymph nodes were selected by size and excised for histological evaluation. Lymph nodes larger than 3 mm in longitudinal diameter were all positive for tumor metastasis, whereas smaller ones exhibited lower positivity (Fig. 5A).

Effect of VEGF-C on lymph node metastasis. The results of the third and fourth series revealed a significant increase in the number of metastases when VEGF-C was overexpressed by the cells (1.1 ± 0.8 *vs* 3.2 ± 1.3, third and fourth series, respectively). Statistical significance was determined by the Mann-Whitney *U*-test (Fig. 5B).

Reproducibility of lymph node metastasis. As shown in Table 1, the majority of animals developed lymph node metastasis at 8 weeks after injection. The overall rate of positive lymph node metastasis was 86.5% (45/52 animals). All lymph nodes >3 mm in longitudinal diameter contained tumor cells, as determined by histological analysis (Fig. 5B). No animals exhibited direct invasion of the tumor or metastatic lesions other than the lymph nodes.

Lymphangiogenesis in the subcutaneous tumor. After 2 weeks of subcutaneous inoculation, the tumors were analyzed histochemically. The tumor tissue based on the HEC1A/VEGF-C cells exhibited a marked increase in VEGFR3-positive vessels compared with the HEC1A/LUC cells (Fig. 6A,B). The number

Table 1. Number of animals with lymph node metastasis

Weeks	4	6	8
First series (HEC1A/LUC)	1/5	2/4	4/4
Second series (HEC1A/LUC)	–	–	8/8
Third series (HEC1A/LUC)	–	–	15/21
Fourth series (HEC1A/VEGF-C)	–	–	18/19

HEC1A, an endometrial cancer cell line; LUC, luciferase; VEGF-C, vascular endothelial growth factor-C.

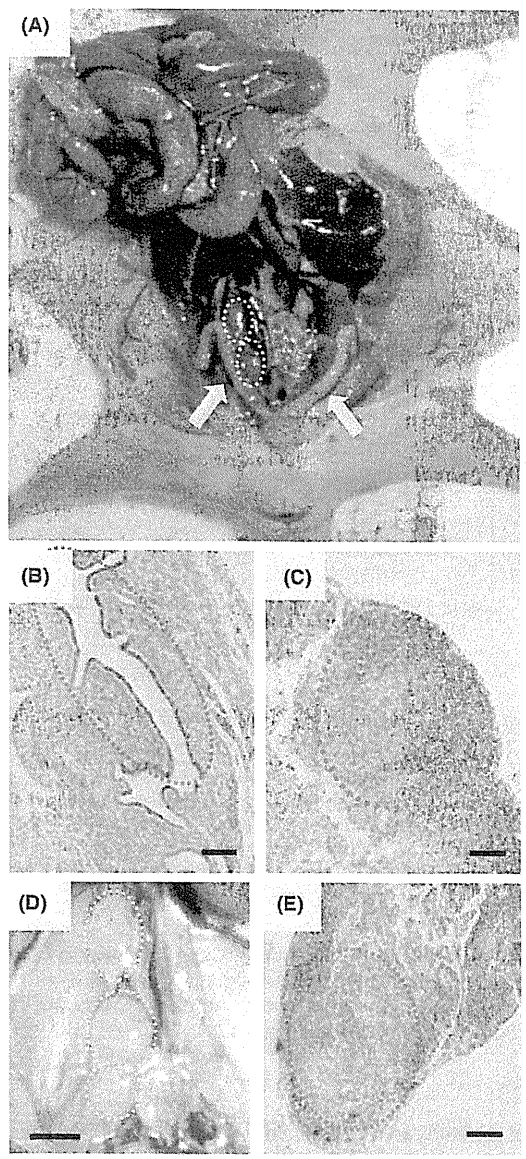

Fig. 4. Involvement of cancer cells *in vivo*, 8 weeks after injection. (A–C) animals were injected with HEC1A/luciferase cells. (A) Enlarged uterus (arrows) and lymph nodes (dotted circles) are shown. No other metastatic sites were found in these animals. (B) Micrograph of a uterus. Tumor cells in the endometrial zone, which resemble a uterus with endometrial cancer. (C) Enlarged lymph node with tumor metastasis. (D) Para-aortic lymph node swelling was observed in mice injected with HEC1A/vascular endothelial growth factor-C cells. Dotted circles indicate enlarged lymph nodes. (E) Lymph node metastasis was confirmed by histological evidence of tumor infiltration. Bars in (B), (C), and (E) indicate 1 mm; bar in (D) indicates 4 mm.

doi: 10.1111/j.1349-7006.2011.02099.x

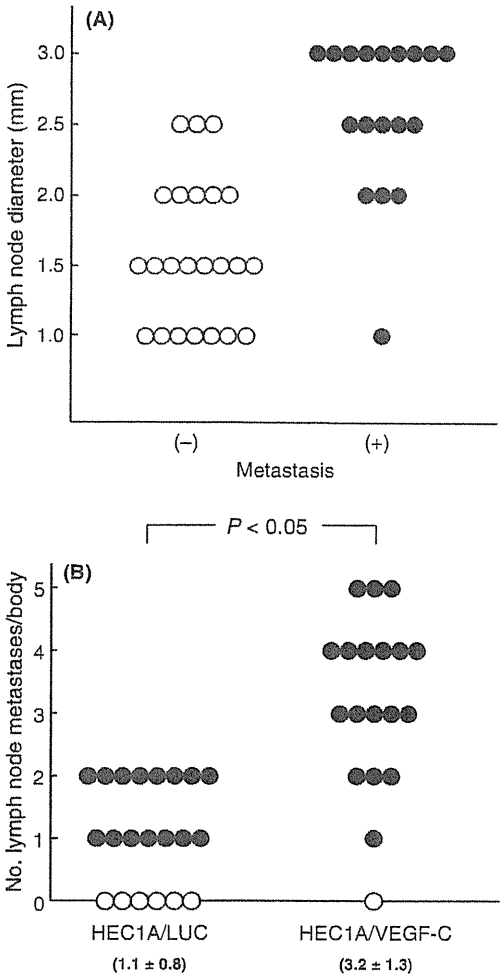

Fig. 5. Number of lymph nodes in animals, 8 weeks after tumor injection. (A) Relationship between lymph node size (longitudinal diameter) and metastasis is shown. Closed circles indicate histologically-positive metastasis. (B) Number of metastatic lymph nodes larger than 3 mm in longitudinal diameter at 8 weeks. Results from the third and fourth series are shown. Closed circles indicate histologically-positive metastasis. Animals injected with HEC1A/vascular endothelial growth factor-C (VEGF-C) showed a higher number of lymph node metastases. LUC, luciferase.

of VEGFR3-positive vessels in each group (n = 4) were counted using microscopy, and the results were analyzed. A significant increase was observed in tumors originated from HEC1A/VEGF-C cells (Student's t-test, Fig. 6C).

Discussion

In the present study, we developed a unique lymph node metastasis model by orthotopically injecting endometrial cancer cells. In this method, most of the animals exhibited lymph node metastasis, along with uterine involvement in cancer. The reproducibility of the metastases seen in our experiment is extremely

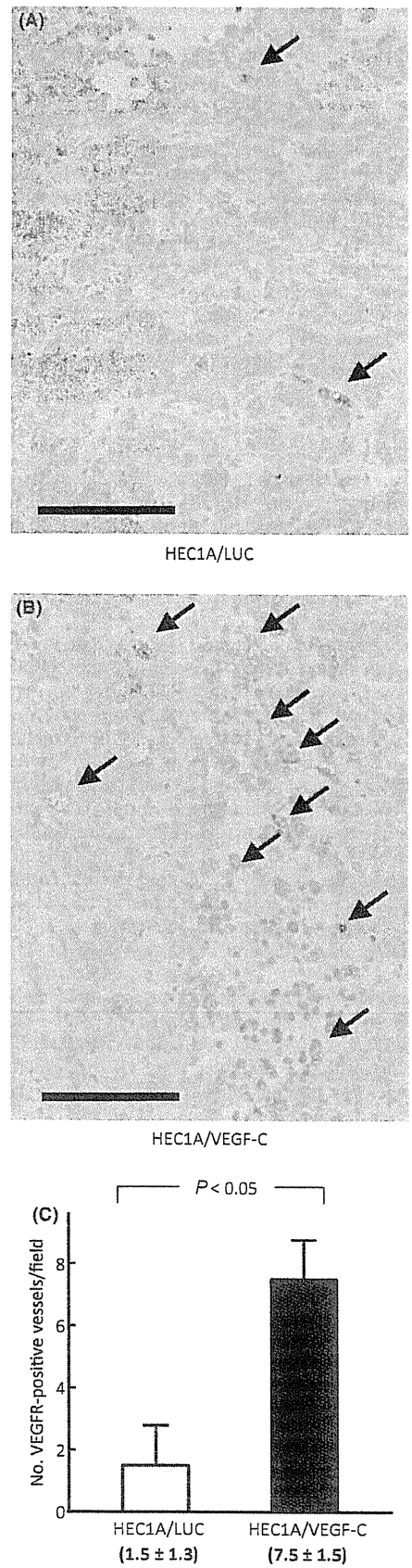

Fig. 6. Immunohistochemical analysis of subcutaneously-inoculated tumor. Arrows indicate vascular endothelial growth factor (VEGF) receptor 3 (VEGFR3)-positive vessels, possibly reflecting lymphangiogenesis in HEC1A/luciferase (LUC) (A) and HEC1A/VEGF-C cells (B). Bars indicate 100 μm. (C) Number of vessels positive for VEGFR3 was enumerated under a light microscope at ×20 magnification. Four animals were used for each cell.

important in developing a model for lymph node metastasis. In our model, all animals survived the injection procedure, and 45 of 52 mice (86.5%) exhibited positive lymph node metastasis. This rate is remarkably high, thus making this model reliable for further therapeutic interventions. In all of the animals, uterine tumor growth was local and self-limited, and the peritoneal dissemination of other sites of metastasis was not evident. These features considerably reflect the clinical conditions of lymph node metastasis, assuring the utility of the model.

Nonetheless, when the present pathological findings are compared to those of human cases, there are slight differences in the metastatic regions. In the mice used in the present experiments, only para-aortic lymph node areas were involved, whereas in humans, pelvic lymph nodes are also metastasized. While this difference might be due to differences in lymphatic anatomy, it would be advantageous for researchers to evaluate metastatic conditions more clearly.

There are a number of decisions to be made when developing models, such as choosing cell lines, the number of cells for injection, various technical details, and observation periods. We initially selected HEC1A cells, because they are one of the most widely used endometrial cancer cell lines. Based on our experience, HEC1A cells appeared to be the most suitable for the present study; lymph node metastasis was well developed before other potential metastatic sites or original growths. One of the most important aspects is the invasiveness of the cells. HEC1A cells are not very invasive by nature, and did not cause peritoneal dissemination in our series of experiments during the observation period. In fact, we also tested HEC50B cells and found that although metastatic lesions were found earlier (by 4–5 weeks), tumor invasion into the surrounding areas was prominent, and consequently, the animals were not suitable for further evaluation of metastasis. The invasiveness seems unrelated to the levels of VEGF-C production, but related to the state of differentiation. HEC1A cells are known to be well differentiated, whereas HEC50B cells are poorly differentiated. In this respect, Ishikawa (3H12) cells might be a good candidate, as they are classified as well-differentiated carcinoma; nonetheless, they are also known to transform into undifferentiated status under prolonged culture.[11] For this reason, we did not test this cell line for the development of the model.

The number of cells per injection is another important factor when developing a model. As a general rule, the more cells that are injected, the earlier the disease develops. The number of cells used in this study (5×10^6) was near maximum, because the least amount of solution to suspend the cells is close to the maximum volume for intrauterine injections in BALB/c mice (approximately 80 μL). It is also imperative to keep the tumor cells within the uterine cavity after injection. To do so, it is important that the distal ends of the uterus and cervix are appropriately ligated, while avoiding excessive amounts of injection. If the cells flow out from the distal end of the uterus, they might spread into the peritoneal space, leading to intraperitoneal tumor dissemination. Alternatively, if the cells are lost through the vagina, the inoculation is deemed unsuccessful. In our experiments, no significant intraperitoneal regions were observed in the animals, even when lymph node metastases were not evident.

Two previous studies established lymph node metastasis models by injecting cancer cells into the uterus. The first study utilized the metastatic subline PL3 of rat Walker 256 cells.[15] This cell line originates from mammary tumor cells, and the metastatic subline was enriched after more than five cycles of *in vivo* selection. Another study orthotopically implanted MH and KF cells; both originate from human ovarian cancer.[16] The latter study also established highly metastatic sublines (MH–LN3 and KF–LN3) after three cycles of *in vivo* selection. Therefore, the *in vivo* selection of the cells is essential before establishing a metastasis model. Meanwhile, the stability of the metastatic sublines, along with their availability, is not clear. In this study, we utilized publicly-available cell lines without *in vivo* selection steps. These features, along with the high rate of reproducibility, make this model particularly useful for evaluating lymph node metastasis.

At the time of histological evaluation, various sizes of lymph nodes were found, and it was difficult to estimate whether they were metastatic or not. To simplify the evaluation steps, we tested for the presence of metastatic tumors in lymph nodes by size. As shown in Figure 5(A), all lymph nodes larger than 3 mm were positive for metastasis. Therefore, we enumerated lymph nodes by using this size limit. In addition, the lymph nodes shown in Figure 5(B) were also analyzed; the additional 84 lymph nodes were all positive for metastasis. With these results, we are confident that we can estimate the metastasis solely by the size of the lymph node, at least in this model.

Based on our results, it is clear that the overexpression of VEGF-C results in an enhancement of lymph node metastasis (Fig. 5B). The use of this particular cell line results in a more robust model for lymph node metastasis. It is very likely that the activity of VEGF-C secreted from the tumors facilitates lymph node metastasis. In the present study, we demonstrated significant increase of VEGFR3-positive vessels within the tumor, suggesting enhanced lymphangiogenesis by VEGF-C (Fig. 6). The precise mechanism of VEGF-C, with regard to lymph node metastasis, is not well understood; few existing studies focus on this point. One study suggests that lymphatic endothelial cell (LEC) migration, rather than proliferation, is responsible for metastasis in pancreatic cell lines.[17] In that study, the relationship between VEGF-C concentration and the number of migrating LEC exhibited a positive but non-linear correlation; this is quite similar to our observation between VEGF-C and the number of lymph node metastases. In any case, it is expected that blocking the activity of VEGF-C would suppress lymph node metastasis. We are currently preparing a therapeutic experiment that incorporates soluble VEGFR3 into this model.

The prognosis of endometrial carcinoma with lymph node metastasis is poor, and few improvements have been made. The present model might offer a platform on which therapeutic progress against lymph node metastasis can be made.

Acknowledgments

This study was supported in part by grants from Ministry of Health, Labor and Welfare, Japan, and the Ministry of Education, Culture, Sports, Science, and Technology, Japan.

Disclosure Statement

The authors declare no financial or commercial conflict of interest.

References

1 Jemal A, Siegel R, Xu J, Ward E. Cancer statistics, 2010. *CA Cancer J Clin* 2010; **60**: 277–300.
2 Lurain JR, Rice BL, Rademaker AW, Poggensee LE, Schink JC, Miller DS. Prognostic factors associated with recurrence in clinical stage I adenocarcinoma of the endometrium. *Obstet Gynecol* 1991; **78**: 63–9.
3 Wolfson AH, Sightler SE, Markoe AM *et al.* The prognostic significance of surgical staging for carcinoma of the endometrium. *Gynecol Oncol* 1992; **45**: 142–6.
4 Hirai M, Nakagawara A, Oosaki T, Hayashi Y, Hirono M, Yoshihara T. Expression of vascular endothelial growth factors (VEGF-A/VEGF-1 and VEGF-C/VEGF-2) in postmenopausal uterine endometrial carcinoma. *Gynecol Oncol* 2001; **80**: 181–8.

doi: 10.1111/j.1349-7006.2011.02099.x

5 Makinen T, Veikkola T, Mustjoki S *et al.* Isolated lymphatic endothelial cells transduce growth, survival and migratory signals via the VEGF-C/D receptor VEGFR-3. *EMBO J* 2001; **20**: 4762–73.
6 Mandriota SJ, Jussila L, Jeltsch M *et al.* Vascular endothelial growth factor-C-mediated lymphangiogenesis promotes tumour metastasis. *EMBO J* 2001; **20**: 672–82.
7 Skobe M, Hawighorst T, Jackson DG *et al.* Induction of tumor lymphangiogenesis by VEGF-C promotes breast cancer metastasis. *Nat Med* 2001; **7**: 192–8.
8 Tanabe H, Takada Y, Minegishi D, Kurematsu M, Masui T, Mizusawa H. Cell line individualization by STR multiplex system in the cell bank found cross contamination between ECV304 and EJ-1/T24. *Tiss Cult Res Commun* 1999; **18**: 329–38.
9 Kuramoto H, Tamura S, Notake Y. Establishment of a cell line of human endometrial adenocarcinoma *in vitro*. *Am J Obstet Gynecol* 1972; **114**: 1012–9.
10 Suzuki M, Kuramoto H, Hamano M, Shirane H, Watanabe K. Effects of oestradiol and progesterone on the alkaline phosphatase activity of a human endometrial cancer cell-line. *Acta Endocrinol (Copenh)* 1980; **93**: 108–13.
11 Nishida M. The Ishikawa cells from birth to the present. *Hum Cell* 2002; **15**: 104–17.
12 Urabe M, Hasumi Y, Ogasawara Y *et al.* A novel dicistronic AAV vector using a short IRES segment derived from hepatitis C virus genome. *Gene* 1997; **200**: 157–62.
13 Takei Y, Mizukami H, Saga Y *et al.* Suppression of ovarian cancer by muscle-mediated expression of soluble VEGFR-1/Flt-1 using adeno-associated virus serotype 1-derived vector. *Int J Cancer* 2007; **120**: 278–84.
14 Kung AL, Wang S, Klco JM, Kaelin WG, Livingston DM. Suppression of tumor growth through disruption of hypoxia-inducible transcription. *Nat Med* 2000; **6**: 1335–40.
15 Hashii K, Tohya K, Kimura M *et al.* Novel animal model of lymph node metastasis by intrauterine inoculation of the actively metastatic subline PL3 separated from rat Walker 256 tumor cells. *Invasion Metastasis* 1997; **17**: 149–57.
16 Tamada Y, Aoki D, Nozawa S, Irimura T. Model for paraaortic lymph node metastasis produced by orthotopic implantation of ovarian carcinoma cells in athymic nude mice. *Eur J Cancer* 2004; **40**: 158–63.
17 Ochi N, Matsuo Y, Sawai H *et al.* Vascular endothelial growth factor-C secreted by pancreatic cancer cell line promotes lymphatic endothelial cell migration in an *in vitro* model of tumor lymphangiogenesis. *Pancreas* 2007; **34**: 444–51.

Journal of Stem Cells & Regenerative Medicine
ISSN 0973 - 7154

RESEARCH ARTICLE

JSRM Code: 007020300010

Reciprocal upregulation of Notch signaling molecules in hematopoietic progenitor and mesenchymal stromal cells

Kikuchi Y[1,2], Kume A[2*], Urabe M[2], Mizukami H[2], Suzuki T[1], Ozaki K[1], Nagai T[1], Ozawa K[1,2]

Although mesenchymal stem cells (MSCs) play pivotal supportive roles in hematopoiesis, how they interact with hematopoietic stem cells (HSCs) is not well understood. We investigated the interaction between HSCs and surrogate MSCs (C3H10T1/2 stromal cells), focusing on the molecular events induced by cell contact of these bipartite populations. C3H10T1/2 is a mesenchymal stromal cell line that can be induced to differentiate into preadipocytes (A54) and myoblasts (M1601). The stromal cell derivatives were cocultured with murine HSCs (Lineage$^-$Sca1$^+$), and gene expression profiles in stromal cells and HSCs were compared before and after the coculture. HSCs gave rise to cobblestone areas only on A54 cells, with ninefold more progenitors than on M1601 or undifferentiated C3H10T1/2 cells. Microarray-based screening and a quantitative reverse transcriptase directed-polymerase chain reaction showed that the levels of Notch ligands (Jagged1 and Delta-like 3) were increased in A54 cells upon interaction with HSCs. On the other hand, the expression of Notch1 and Hes1 was upregulated in the HSCs cocultured with A54 cells. A transwell assay revealed that the reciprocal upregulation was dependent on cell-to-cell contact. The result suggested that in the hematopoietic niche, HSCs help MSCs to produce Notch ligands, and in turn, MSCs help HSCs to express Notch receptor. Such a reciprocal upregulation would reinforce the downstream signaling to determine the fate of hematopoietic cell lineage. Clarification of the initiating events on cell contact should lead to the identification of specific molecular targets to facilitate HSC engraftment in transplantation therapy.

Introduction

Hematopoietic stem cells (HSCs) are capable of self-renewing and differentiating into all the blood cell lineages, and the property allows them to reconstitute adult hematopoiesis following transplantation. The growth and differentiation of HSCs is regulated by orchestrated signals from various soluble factors and the hematopoietic microenvironment, or 'niche'. With the aid of many other cell types, osteoblasts and vascular endotherial cells maintain the balance of dormant and active HSCs in the osteoblasic and vascular niches [1-4].

The interaction between HSCs and the niche cells comprises cytokines and cell-to-cell contact. The involved cytokines include stem cell factor (SCF), stromal-derived factor 1 (SDF1), angiopoietin1 (Ang1) and osteopontin, and the functions of these factors have been studied extensively [5-9]. On the other hand, molecular events of the direct cell contact are mostly unclear. Wagner et al. investigated the behavioral and molecular changes in hematopoietic progenitors upon interaction with a stromal cell line AFT024 [10]. They found that the genes involved in the cytoskeleton reorganization, DNA stabilization and methylation were upregulated. However, molecular events in the niche cells have not vigorously explored.

Mesenchymal stem cells (MSCs) in the bone marrow play a vital role in supporting hematopoiesis, therefore they are considered as niche cells, too [11,12]. To further explore the hematopoiesis-supporting ability of MSCs, we have used a surrogate MSC line C3H10T1/2 (10T1/2) and its derivative preadipocytes (A54) and myoblasts (M1601). Among these cells, only A54 preadipocytes helped the expansion of hematopoietic progenitors with an augmented production of SCF, SDF1 and Ang1 [13,14]. In the present study, we investigated the cellular and molecular events in the interactive communication between HSCs and stromal cells using this differentiation-inducible system, particularly focusing on the changes in the stromal cells.

Materials and methods

Cells

10T1/2 cell line (from Riken Biological Resource Center, Tsukuba, Japan) was used as an inducible MSC model. A54 preadipocytes and M1601 myoblasts were established as described previously [13]. All the cell lines were cultured in Iscove's Modified Dulbecco's Medium (Invitrogen, Carlsbad, CA, USA) supplemented with 10% fetal bovine serum (FBS; Sigma, St. Louis, MO, USA). Bone marrow mononuclear cells were separated from C57BL/6 mouse femurs using

[1]Division of Hematology, Department of Medicine, Jichi Medical University, Shimotsuke, Tochigi, Japan.
[2]Division of Genetic Therapeutics, Center for Molecular Medicine, Jichi Medical University, Shimotsuke, Tochigi, Japan.

Received 02 Jun; accepted 23 Jul; published online 30Oct 2011

Lympholyte-M (Cedarlane, Hornby, ON, Canada), and serially fractionated with immunomicrobeads and AutoMACS (Miltenyi Biotech, Bergisch Gradbach, Germany). Lineage-negative (Lin^-) and –positive (Lin^+) cells were separated with a Lineage Cell Depletion Kit (Miltenyi Biotech). Sca1-, CD45R (B220)- and CD90 (Thy1.2)-positive cells ($Sca1^+$, $B220^+$ and $Thy1.2^+$ cells, respectively) were separated with appropriate microbeads (Miltenyi Biotech). Lin^-Sca1^+ cells were used as HSCs. Lin^+B220^+ cells and $Lin^+Thy1.2^+$ cells were used as B-lymphocytes and T-lymphocytes, respectively.

Coculture of HSCs and stromal cells

10T1/2, A54 and M1601 stromal cells were inoculated (5 x 10^3 cells/well) on a 12-well culture plate (Falcon 3043, BD, Franklin Lakes, NJ, USA). After 2 days, the near-confluent cells (ca. 2 x 10^4 cells/well) were gamma-irradiated (30 Gy) using a Gammacell 40 Exactor (Nordion International, Ottawa, ON, Canada) to prevent hyperproliferation. Then 1 x 10^4 HSCs (Lin^-Sca1^+ cells) were added to the irradiated stromal cells and cocultured for 5 days in α-Minimum Essential Medium (Invitrogen) supplemented with 10% FBS. A coculture was also carried out using a Cell Culture Insert (Falcon 353090, BD) on a 6-well culture plate (Falcon 3046, BD) for 5 days, with HSCs seeded in the upper wells and stromal cells in the lower wells. After coculture, cells were examined for cobblestone formation (30 or more clustered HSCs) on an inverted fluorescent microscope (Olympus IX-70, Tokyo, Japan), and the stromal cells and HSCs were separated with MACSelect K^k microbeads (Miltenyi Biotech) and AutoMACS for further analyses. The stromal cells derived from C3H mouse ($H\text{-}2^k$) were separated as a positive fraction, and HSCs derived from C57BL/6 mouse ($H\text{-}2^b$) were separated as a negative fraction. The separated cells were stained with a phycoerythrin-conjugated anti-mouse $H\text{-}2K^k$ antibody and a fluorescein isothiocyanate-conjugated anti-mouse $H\text{-}2K^b$ antibody (BD Biosciences, San Jose, CA, USA), and the purity was evaluated with BD LSR and CellQuest software (BD Immunosystems, Mountain View, CA, USA). For colony asaay after coculture, separated HSCs were cultivated (1 x 10^3 cells/35 mm dish) in growth factor-containing methylcellulose medium (MethoCult GF M3434, StemCell Technologies, Vancouver, BC, Canada) and colonies were counted on day 7.

Gene expression analysis

To quantify several signaling molecules, the reverse transcriptase-directed polymerase chain reaction (RT-PCR) was performed. Total RNA was extracted from the cells using an RNeasy Mini Kit (QIAGEN, Hilden, Germany), and cDNA was synthesized with a SuperScript First-Strand Synthesis Kit (Invitrogen). PCR was carried out with a QuantiTect SYBR Green PCR Kit (QIAGEN), and the incorporation of the fluorescent dye into the PCR products was monitored with ABI Prism 7700 (Applied Biosystems, Foster City, CA, USA). As internal controls, beta-actin was used for the stromal cells and glyceraldehyde-3-phosphate dehydrogenase was used for HSCs. The primers for PCR are listed in Table 1. Gene expression profiles of A54 before and after coculture with HSCs were compared using a FilgenArray Mouse 32K (Filgen, Nagoya, Japan).

Table 1. RT-PCR primer design.

Target	Forward primer	Reverse primer
Ang1	CCAATCTAAATGGAATGTTCT	CAGAGCACCTTCAAAAGTCCA
beta-actin	CCATCATGAAGTGTGACGTTG	GTCCGCCTAGAAGCACTTGCG
BMP6	TTCTCCCCACATCAACGACACC	AAACTCCCCACCACACAGTCC
Dll3	CCAGTAGCTGCCTGAACTCC	ATTGAAGCAGGGTCCATCTG
GAPDH	CCTGGAGAAACCTGCCAAGTATG	AGAGTGGGAGTTGCTGTTGAAGTC
Hes1	AAAGCCTATCATGGAGAAGAGGCG	GGAATGCCGGGAGCTATCTTTCTT
Jag1	CCGTAATCGCATCGTACTGC	GGCCTCCACCAGCAAAGTGT
Notch1	TGTTAATGAGTGCATCTCCAACCCA	CATTCGTAGCCATCAATCTTGTCC
SCF	ATGGACAGCCATGGCATTGC	CACCTCTTGAAATTCTCTCT
SDF1	GCCCTTCAGATTGTTGCA	CGTCTGACTCACACCTCACA

Immunostaining

A54 cells and HSCs were cocultured on Culture Slides (Falcon 354111, BD), and immunostained on day 5. The cells were fixed with 4% paraformaldehyde, and incubated with a rabbit anti-mouse Jag1 antibody (ab7771, Abcam, Cambridge, UK) and Alexa Fluor 488-conjugated goat anti-rabbit IgG (A11008, Invitrogen) for 30 minutes on ice, respectively. Slides were inspected and photographed under an IX-70 microscope.

Statistical analysis

The statistical analysis was performed using a Statcel2 (OMS Publishing, Saitama, Japan) add-on package for Microsoft Excel. Student's t-test was used for comparison between two groups, and a multiple comparison test (the Turkey-Kramer method) was used for comparison among groups of three or more. A P-value < 0.05 was considered to be significant for all analyses.

Results

Requirement of cell contact in supporting hematopoeisis

In coculure experiments with 10T1/2 or its derivatives (A54 and M1601), HSCs formed cobblestone areas only on A54 at day 5 (12.5 ± 0.6 cobblestone areas/10^4 cells), as we reported previously [14]. We also confirmed that the murine hematopoietic progenitors were expanded by ninefold (36.0 ± 4.0 colonies/10^3 cells post-coculture with A54 vs. 4.0 ± 2.0 colonies/10^3 cells pre-coculture, Figure 1) whereas the number of hematopoietic progenitors was not significantly increased after the coculture with parental 10T1/2 cells or M1601 myoblasts (3.3 ± 1.5 colonies/10^3 cells with 10T1/2, and 6.3 ± 1.5 colonies/10^3 cells with M1601; Figure 1). Without stromal cell support, HSCs completely lost their progenitor activity in the same medium used for coculture ('No stroma' in Figure 1). Indeed, only few monocyte/macrophage-like cells were found after 5-day-incubation in this population; we speculated that all the clonogenic cells fell into apoptosis because no additional cytokine was provided. As we previously reported, expression of SCF, SDF1 and Ang1 in A54 was greater than that in 10T1/2 and M1601cells [14]. Such an overexpression of SCF, SDF1 and Ang1 in A54 cells was not further augmented or cancelled by addition of interleukin-1 or coculture with HSCs (data not shown).

Next, we addressed whether soluble factors from A54 preadipocytes were sufficient for supporting hematopoiesis. To discriminate the contribution of cell communication via direct adhesion, mouse bone marrow-derived HSCs were cultivated on a microporous membrane (1 micron Cell Culture Insert) placed in a well containing A54 cells underneath. We found that physical separation from A54 cells totally abrogated the progenitor activity of HSCs, in spite of the availability of soluble molecules from the stromal cells (Figure 1). This observation indicated that A54 cells supported hematopoiesis by cell contact in addition to secreting cytokines.

Gene expression changes in preadipocytes cocultured with HSCs

Upon learning that cell adhesion is required for A54 cells to support HSCs, we speculated that some signaling from HSCs to stromal cells might occur during coculture. This idea prompted us to search for molecules whose expression changed in A54 cells cocultured with HSCs. Total RNA was extracted from A54 cells before and after the coculture and gene expression profiles were compared by microarray. Out of 33696 genes screened, 353 genes were upregulated by twofold or more after the coculture with HSCs, and 13 genes were downregulated to the levels less than a half of starting value (data not shown). Among them, 29 genes (21 upregulated and 8 downregulated; Table 2) were implicated to be involved in hematopoiesis. Therefore we focused on these molecules for further investigation. A quantitative RT-PCR analysis confirmed the upregulation of Jagged 1 (Jag1), Delta-like 3 (Dll3) and bone morphogenetic protein 6 (BMP6) in A54 cells after coculture with HSCs (Figure 2). On the other hand, upregulation of Jag1, Dll3 and BMP6 was not observed in the undifferentiated 10T1/2 cells or M1601 myoblasts after coculture with HSCs (data not shown). Expression of Jag1 was also increased in A54 cells cultured with differentiated cells such as B- and T-lymphocytes, but to a lesser extent (Figure 2A).

Figure 1

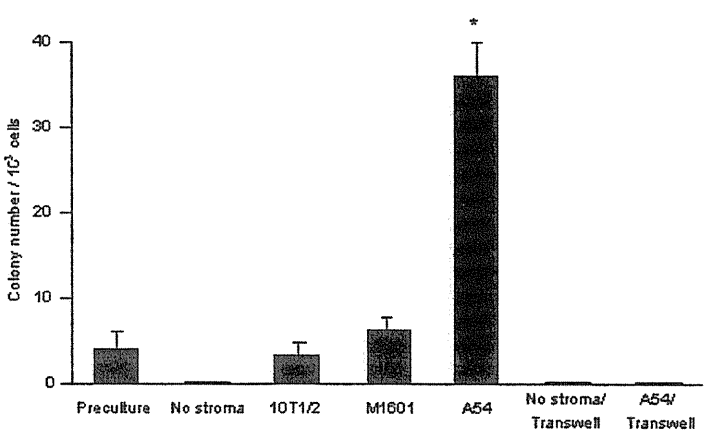

Figure 1. Requirement of direct contact for preadipocytes to support hematopoiesis. 1 x 10^4 mouse bone marrow Lin^-Sca1^+ cells (HSCs) were cocultured with 2 x 10^4 C3H10T1/2 cells (10T1/2), 10T1/2-derived myoblasts (M1602) or preadipocytes (A54) for 5 days. After coculture, HSCs were separated with immunomagnetic beads and subjected to colony assay. HSCs were seeded on MethoCult GF M3434 (1 x 10^3 cells/dish) and colonies were counted on day 7. Preculture: colonies from HSCs prior to coculture. No stroma: colonies from HSCs incubated 5 days without stromal support. No stroma/Transwell: colonies from HSCs seeded on the top wells, with no stromal cells in the bottom wells. A54/Transwell: HSCs were coincubated with A54 but separated by Cell Culture Insert. *: P < 0.01 (n = 3).

Figure 2

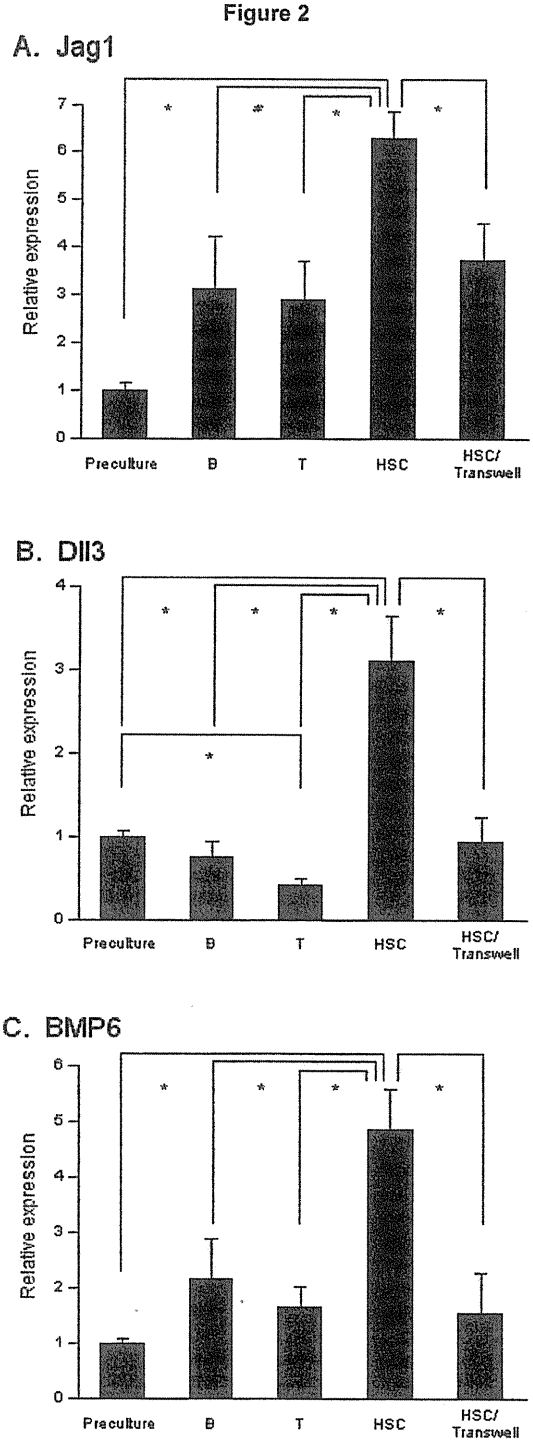

Figure 2. Elevated levels of Jag1, Dll3 and BMP6 in A54 cells cocultured with HSCs. Total RNA was isolated from 2 x 10^4 A54 cells prior to coculture (Preculture) and after 5-day-coculture with 1 x 10^4 B-lymphocytes (B), 1 x 10^4 T-lymphocytes (T) or 1 x 10^4 bone marrow Lin^-Sca1^+ cells (HSC). Expression of Jag1 (A), Dll3 (B) and BMP6 (C) was measured by quantitative RT-PCR with the primers listed in Table 1. HSC/Transwell: A54 cells were coincubated with HSCs but separated by Cell Culture Insert. *: $P < 0.01$ ($n = 3$).

Dll3 expression in A54 was decreased after coculture with T-cells, while it was not significantly changed after coculture with B-cells (Figure 2B). BMP6 expression was mildly upregulated in A54 cells cocultured with mature lymphocytes, but the difference was not statistically significant (Figure 2C). These results suggested that the upregulation of Jag1, Dll3 and BMP6 was induced by interaction with immature hematopoietic cells. Furthermore, such elevation was cancelled out when A54 cells were separated from HSCs with a microporous membrane (Figure 2). Immunostaining with an anti-Jag1 antibody confirmed that hematopoietic progenitors stimulated Jag1 expression in the neighboring A54 preadipocytes. Jag1 signal was apparently greater in A54 cells in cobblestoned areas than those in the surrounding regions (Figure 3). Taken together, mesenchymal stromal cell-derived preadipocytes received signals from HSCs through cell contact, resulting in multiple events including upregulation of Jag1, Dll3 and BMP6.

Activation of Notch signaling in HSCs

The coculture experiment showed that the expression of multiple Notch ligands (Jag1 and Dll3) was upregulated in A54 preadipocytes during their interaction with HSCs. We next addressed whether the expression of Notch receptors and downstream factors was altered in the HSCs.

Figure 3

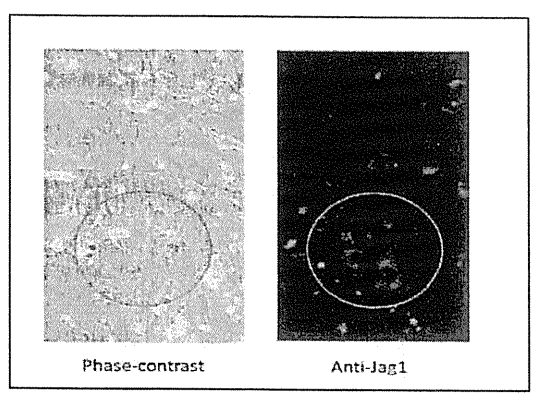

Figure 3. Jag1 expression in a cobblestone area. 1 x 10^4 murine bone marrow HSCs were incubated on 2 x 10^4 A54 cells for 5 days. Cells were immunostained with a rabbit anti-mouse Jag1 antibody and Alexa Fluor 488-conjugated goat anti-rabbit IgG. In the left panel (phase-contrast bright field, magnification × 400), a cobblestone area with small, rounded hematopoietic cells is indicated with a circle. In the right panel (immunofluorescent view, magnification × 400) showing the same location, several large, stretched stromal cells are positively immunostained (green), wheras stromal cells outside the cobblestone area are negative or weakly positive.

Table 2. Hematopoiesis-related genes upregulated or downregulated in cocultured A54 cells.

Upregulated or downregulated molecule	Before [a]	After [b]	Ratio [c]
Upregulated			
Mcl1 (Myeloid cell leukemia sequence 1)	116	514	4.42
Stom (Stomatin)	126	481	3.83
Foxk1 (Forkhead box K1)	129	464	3.58
Foxf2 (Forkhead box F2)	133	455	3.43
Bmp6 (Bone morphogenetic protein-6)	133	451	3.38
Itgbl1 (Integrin , beta-like 1)	135	447	3.30
Dll3 (Delta-like 3)	136	446	3.29
Arts1 (Adipocyte-derived leucine aminopeptidase)	136	446	3.28
Sox13 (SRY-box containing gene 13)	136	444	3.27
Cdc40 (Cell division cycle 40 homolog)	136	443	3.26
Jag1 (Jagged 1)	137	443	3.24
Shh (Sonic hedgehog)	137	440	3.20
Cdc16 (Cell division cycle 16 homolog)	143	423	2.95
Sox17 (SRY-box containing gene 17)	146	416	2.85
Cdc2l6 (Cell division cycle 2-like 6)	144	408	2.83
Col15a1 (procollagen , type XV)	147	408	2.77
Rras (Ras-related protein)	149	405	2.72
Pik3cb (phosphatidylinositol3-kinase, catalytic, b polypeptide)	147	401	2.72
Hoxa3 (Homeobox A3)	149	378	2.54
Adfp (Adipophilin, Adipose differentiation-related protein)	150	361	2.41
Cdc91l1 (cell division cycle 91-like 1)	146	324	2.22
Downregulated			
Nudt2 (nucleoside diphosphate linked moiety X - type motif 2)	3155	1337	0.42
Lrp2 (LDL receptor-related protein 2)	2210	963	0.44
TPO (thrombopoietin)	866	419	0.48
Taar1 (trace amine-associated receptor 1)	892	432	0.48
Centg3 (centaurin , gamma 3)	1932	942	0.49
Ccdc66	777	382	0.49
Olig1 (oligodendrocyte transcription factor 1)	1293	639	0.49
AA474455	1809	897	0.49

[a] Before: Expression (net intensity) in A54 cells before coculture.
[b] After: Expression in A54 cells after 3 days of coculture with HSCs.
[c] Ratio = After/Before.

A quantitative RT-PCR analysis revealed that the message level of Notch1 was elevated in HSCs cocultured with A54 cells by 3.6-fold (Figure 4A). Simultaneously, the expression of Hairy enhancer of split-1 (Hes1), a target of Notch1, was upregulated by 27-fold, indicating that the authentic signaling pathway was actually viable (Figure 4B). The results clearly showed that Notch ligands and receptors were upregulated in the stromal cells and HSCs in a reciprocal fashion through cell contact.

Discussion

In the present study, we investigated the molecular events in hematopoiesis supported by mesenchymal stromal cell-derived preadipocytes. We and other investigators reported that several preadipocyte-like stromal cells were capable of supporting hematopoiesis [13–16]. While osteoblasts enhance HSC self-renewal in the hematopoietic niche [2,3], preadipocytes may have additional or different function, such as promoting the asymmetric division of HSCs and proliferation of early progenitors. Our finding that A54 preadipocytes promoted the formation of cobblestone areas and colonies supports this idea, but such function may not be completely cell-autonomous. Assuming that some instructive signals from HSCs, we investigated the gene expression profile of A54 cells in a coculture with HSCs. Among the molecules upregulated or downregulated by more than twofold in a microarray screening, an increase of Notch ligands (Jag1 and Dll3) and BMP6 was confirmed in A54 cells. This finding is intriguing, because signals from Notch and BMP receptors are integrated in osteoblasts and other cell types [17-20]. Notch is a single-pass transmembrane receptor interacting with cell-bound ligands. So far, four Notch receptors (Notch1-4) and five ligands (Jag1-2 and Dll1, 3 and 4) have been identified in mammals. As in many cell systems, Notch signaling is essential for regulating HSCs and blood cell differentiation [21,22].

Previous studies showed that Jag1 in marrow stromal cells and osteoblasts promotes HSC proliferation [3,23], Dll1 produces cobblestone areas [24]. In the present study, we demonstrated that coculturing resulted in concomitant increases in Notch ligands (Jag1 and Dll3) in A54 preadipocytes and Notch signaling in HSCs. Notably, in accordance with an elevation in levels of the Notch1 receptor, expression of the transcription factor Hes1 was also upregulated. Hes1, one of the targets of Notch signaling, regulates specific groups of genes to maintain HSCs and early progenitors [25,26]. Thus, upregulation of the Notch1-Hes1 axis in HSCs strongly suggests that this signaling pathway is actually viable with the increase in Notch ligands in neighboring preadipocytes. Since Notch activation plus cytokine receptor signaling has a combined effect on hematopoietic cells [27], production of Notch ligands and cytokines (SCF, SDF1 and Ang1) by A54 cells is likely to represent a physiological role of marrow niche cells.

Figure 4

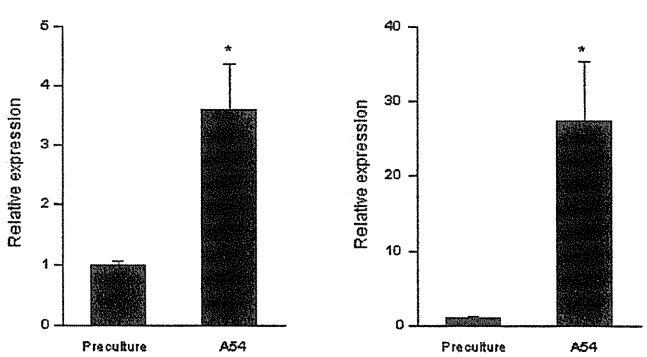

Figure 4. Expression of Notch1 and Hes1 in HSCs. Total RNA was isolated from 1 x 10^4 bone marrow Lin^-Sca1^+ cells prior to coculture and after 5-day-coculture with 2 x 10^4 A54 cells. Notch1 and Hes1 message levels were estimated by quantitative RT-PCR before (Preculture) and after coculture with A54 preadipocyres (A54). The primers for PCR are listed in Table 1. Both Notch1 (A) and Hes1 (B) were significantly upregulated in HSCs after coculture with A54 cells. * : $P < 0.01$ ($n = 4$).

Figure 5

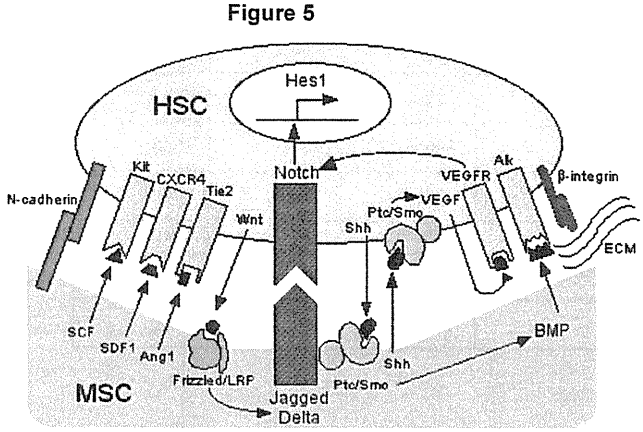

Figure 5. Interaction of MSCs and HSCs. Various factors are involved in the cell-to-cell interaction between MSCs and HSCs with spatial and temporal complexity. HSCs attach to MSCs via adhesion molecules such as N-cadherin and b-integrins (ECM: extracellular matrix secreted from MSC-derived cells). Soluble cytokines from MSCs such as SCF, SDF1 and Ang1 support the growth and differentiation of HSCs through cognate receptors (Kit, CXCR4 and Tie2). When HSCs and MSCs are in close proximity, expression of Notch ligands (Jagged and Delta-like) is upregulated in MSCs by Wnt from HSCs, while that of Notch receptors is upregulated in HSCs by Sonic hedgehog (Shh) from MSCs and HSCs. Vascular endothelial growth factor (VEGF) can further upregulate Notch receptor expression in an autocrine or paracrine fashion. The upregulated Notch signaling pathway induces the expression of downstream targets such as Hes1. The expression of bone morphogenic protein (BMP) is upregulated in MSCs by Shh signaling. Frizzled, Ptc/Smo, VEGFR, Alk: receptors for Wnt, Shh, VEGF and BMP, respectively.

Bone morphogenetic proteins (BMPs) belong to the transforming growth factor-b superfamily and have pleiotropic effects on tissue development. They have been implicated as key regulators in hematopoiesis: for example, BMP4 promotes the self-renewal of HSCs [28] and BMP6 enhances the formation of colonies [17]. Because of the redundancy of ligands/receptors and the dependence on the context and stage of differentiation of target cells, a detailed understanding of BMP signaling awaits further investigation.

The mechanisms responsible for the reciprocal upregulation of the expression of Notch ligands and receptors have yet to be clarified. We found that mature lymphocytes poorly induced Jag1, Dll3 and BMP6 expression in A54 cells, thus the stromal cells appear to receive the induction signal mainly from immature cells such as HSCs. Direct cell-to-cell contact with, or close proximity to HSCs was required for the upregulation of Jag1, Dll3 and BMP6 expression in A54 cells. Thus far several classes of molecules have been implicated to act upstream of Notch signaling. For example, the Wnt canonical pathway regulates the expression of Notch ligands in various cell types [29-31]. Sonic hedgehog (Shh) and receptors for Shh (Ptc/Smo) are expressed on primitive hematopoietic cells and marrow stromal cells and induce BMP expression [32,33]. In addition, Shh can increase levels of Notch receptors via vascular endothelial growth factor (VEGF) [34]. Of note, Wnt and Shh are lipid-modified proteins, and therefore appropriate for exerting effects on short-ranged target cells in a paracrine and/or autocrine fashion [35,36]. In the hematopoietic niche, these signaling networks must be precisely orchestrated to regulate HSC behavior, presumably through cross-talk with signals from adhesion molecules such as integrins (Figure 5). Further investigation of such communicative events will identify target molecules to improve engraftment in transplantation therapy.

References

1. Schofield R. The relationship between the spleen colony-forming cell and the haemopoietic stem cell. Blood Cells 1978; 4: 7-25.
2. Zhang J, Niu C, Ye L, Huang H, He X, Tong W-G, Ross J, Haug J, Johnson T, Feng JQ, Harris S, Wiedemann LM, Mishina Y, Li L. Identification of the haematopoietic stem cell niche and control of the niche size. Nature 2003; 425: 836-841.
3. Calvi LM, Adams GB, Weibrecht KW, Weber JM, Olson DP, Knight MC, Martin RP, Schipani E, Divieti P, Bringhurst FR, Milner LA, Kronenberg HM, Scadden DT. Osteoblastic cells regulate the haematopoietic stem cell niche. Nature 2003; 425: 841-846.
4. Kiel MJ, Yilmaz ÖH, Iwashita T, Yilmaz OH, Terhorst C, Morrison SJ. SLAM family receptors distinguish hematopoietic stem and progenitor cells and reveal endothelial niches for stem cells. Cell 2005; 121: 1109-1121.
5. Heissig B, Hattori K, Dias S, Friedrich M, Ferris B, Hackett NR, Crystal RG, Besmer P, Lyden D, Moore MAS, Werb Z, Rafii S. Recruitment of stem and progenitor cells from the bone marrow niche requires MMP-9 mediated release of Kit-ligand. Cell 2002; 109: 625-637.
6. Ara T, Tokoyoda K, Sugiyama T, Egawa T, Kawabata K, Nagasawa T. Long-term hematopoietic stem cells require stromal cell-derived factor-1 for colonizing bone marrow during ontogeny. Immunity 2003; 19: 257-267.
7. Hattori K, Heissig B, Tashiro K, Honjo T, Tateno M, Shieh J-H, Hackett NR, Quitoriano MS, Crystal RG, Rafii S, Moore MAS. Plasma elevation of stromal cell-derived factor-1 induces mobilization of mature and immature hematopoietic progenitor and stem cells. Blood 2001; 97: 3354-3360.
8. Arai F, Hirao A, Ohmura M, Sato H, Matsuoka S, Takubo K, Ito K, Koh GY, Suda T. Tie2/Angiopoietin-1 signaling regulates hematopoietic stem cell quiescence in the bone marrow niche. Cell 2004; 118: 149-161.
9. Stier S, Ko Y, Forkert R, Lutz C, Neuhaus T, Grünwald E, Chen T, Dombkowski D, Calvi LM, Rittling SR, Scadden DT. Osteopontin is a hematopoietic stem cell niche component that negatively regulates stem cell pool size. J Exp Med 2005; 201: 1781-1791.
10. Wagner W, Saffrich R, Wirkner U, Eckstein V, Blake J, Ansorge A, Schwager C, Wein F, Milesala K, Ansorge W, Ho AD. Hematopoietic progenitor cells and cellular microenvironment: behavioral and molecular changes upon interaction. Stem Cells 2005; 37: 1180-1191.
11. Pittenger MF, Mackay AM, Beck SC, Jaiswal RK, Douglas R, Mosca JD, Moorman MA, Simonetti DW, Craig S, Marshak. Multilineage potential of adult human mesenchymal stem cells. Science 1999; 284: 143-147.
12. Wagner W, Wein F, Roderburg C, Saffrich R, Faber A, Krause U, Schubert M, Benes V, Eckstein V, Maul H, Ho AD. Adhesion of hematopoietic progenitor cells to human mesenchymal stem cells as a model for cell-cell interaction. Exp Hematol 2007; 35: 314-325.
13. Nishikawa M, Ozawa K, Tojo A, Yoshikubo T, Okano A, Tani K, Ikebuchi k, Nakauchi H, Asano S. Changes in hematopoiesis-supporting ability of C3H10TI/2 mouse embryo fibroblasts during differentiation. Blood 1993; 81: 1184-1192.
14. Oh I, Ozaki K, Miyazato A, Sato K, Meguro A, Muroi K, Nagai T, Mano H, Ozawa K. Screening of genes responsible for differentiation of mouse mesenchymal stromal cells by DNA micro-array analysis of C3H10T1/2 and C3H10T1/2-derived cell lines. Cytotherapy 2007; 9: 80-90.
15. Yoshikubo T, Ozawa K, Takahashi K, Nishikawa M, Horiuchi N, Tojo A, Tani K, Kodama H, Asano S. Adhesion of NFS-60 myeloid leukemia cells to MC3T3-G2/PA6 stromal cells induces granulocyte colony-stimulating factor production. Blood 1994; 84: 415-420.
16. Nakamura M, Harigaya K, Watanabe Y. Correlation between production of colony-stimulating activity (CSA) and adipose conversion in a murine marrow-derived preadipocyte line (H-1/A). Proc Soc Exp Biol Med 1985; 179: 283-287.
17. Detmer K, Walker AN. Bone morphogenetic proteins act synergistically with haematopoietic cytokines in the differentiation of haematopoietic progenitors. Cytokine 2002; 17: 36-42.
18. Nobta M, Tsukazaki T, Shibata T, Xin C, Moriishi T, Sakano S, Shindo H, Yamaguchi A. Critical regulation of bone morphogenic protein-induced osteoblastic differentiation by Delta1/Jagged1-activated Notch1 signaling. J Biol Chem 2005; 280: 15842-15848.
19. Katoh M, Katoh M. Transcriptional regulation of WNT2B based on the balance of Hedgehog, Notch, BMP and WNT signals. Int Natl J Oncol 2009; 34: 1411-1415.
20. Blank U, Karlsson S. Signaling pathways governing cell fate. Blood 2009; 111: 492-503.
21. Chiba S. Notch signaling in stem cell systems. Stem Cells 2006; 24: 2437-2447.

22. Weber JM, Calvi LM. Notch signaling and the bone marrow hematopoietic stem cell niche. Bone 2010; 46: 281-285.
23. Duncan AW, Rattis FM, DiMascio LN, Congdon KL, Pazianos G, Zhao C, YoonK, Cook JM, Willert K, Gaiano N, Reya T. Integration of Notch and Wnt signaling in hematopoietic stem cell maintenance. Nature Immunol 2005; 6: 314-322.
24. Moore KA, Pytowski B, Witte L, Hicklin D, Lemischka I. Hematopoietic activity of a stromal cell transmembrane protein containing epidermal growth factor-like repeat motifs. Proc Natl Acad Sci USA 1997; 94: 4011-4016.
25. Kunisato A, Chiba S, Nakagami-Yamaguchi E, Kumano K, Saito T, Masuda S, Yamaguchi T, Osawa M, Kageyama R, Nakauchi H, Nishikawa M, Hirai H. HES-1 preserves purified hematopoietic stem cell ex vivo and accumulates side population cells in vivo. Blood 2003; 101: 1777-1783.
26. Yu X, Alder JK, Chun JH, Friedman AD, Heimfeld S, Cheng L, Civin CI. HES1 inhibits cycling of hematopoietic progenitor cells via DNA binding. Stem Cells 2006; 24: 876-888.
27. Varnum-Finney B, Xu L, Brashem-Stein C, Nourrigat C, Flowers D, Bakkour S, Pear WS, Bernstein ID. Pluripotent, cytokine-dependent, hematopoietic stem cells are immortalized by constitutive Notch1 signaling. Nat Med 2000; 6: 1278-1281.
28. Bhatia M, Bonnet D, Wu D, Murdoch B, Wrana J, Gallacher L, Dick JE. Bone morphogenetic proteins regulate the developmental program of human hematopoietic stem cells. J Exp Med 1999; 189: 1139-1148.
29. Murdoch B, Chadwick K, Martin M, Shojaei F, Shah KV, Gallacher L, Moon RT, Bhatia M. Wnt-5A augments repopulating capacity and primitive hematopoietic development of human blood stem cells in vivo. Proc Natl Acad Sci USA 2003; 100: 3422-3427.
30. Katoh M, Katoh H. Notch ligand, JAG1, is evolutionarily conserved target of canonical WNT signaling pathway in progenitor cells. Int J Mol Med 2006; 17: 681-685.
31. Estrach S, Ambler CA, Lo Celso C, Hozumi K, Watt FM. Jagged 1 is a b-catenin target gene required for ectopic hair follicle formation in adult epidermis. Development 2006; 133: 4427-4438.
32. Bhardwaj G, Murdoch B, Wu D, Baker DP, Williams KP, Chadwick K, Ling LE, Karanu FN, Bhatia M. Sonic hedgehog induces the proliferation of primitive hematopoietic cells via BMP regulation. Nat Immunol 2001; 2: 172-180.
33. Katoh Y, Katoh M. Hedgehog signaling pathway and gastrointestinal stem cell signaling network (review). Int J Mol Med 2006; 18: 1019-1023.
34. Lawson ND, Vogel AM, Weinstein BM. Sonic hedgehog and vascular endothelial growth factor act upstream of the notch pathway during arterial endothelial differentiation. Dev Cell 2002; 3: 127-136.
35. Willert K, Brown JD, Danenberg E, Duncan AW, Weissman IL, Reya T, Yates JR III, Nusse R. Wnt proteins are lipid-modified and can act as stem cell growth factors. Nature 2003; 423: 448-452.
36. Porter JA, Young KE, Beachy PA. Cholesterol modification of Hedgehog signaling proteins in animal development. Nature 1996; 274: 255-259.

Grants

This work was supported in part by grants-in-aid for scientific research from the Ministry of Health, Labour and Welfare, and the Ministry of Education, Culture, Sports, Science and Technology of Japan.

Correspondence to be addressed to:

* Akihiro Kume, M.D., Ph.D., Division of Genetic Therapeutics, Center for Molecular Medicine, Jichi Medical University. 3311-1 Yakushiji, Shimotsuke, Tochigi 329-0498, Japan. Tel: +81-285-58-7402; Fax: +81-285-44-8675; Email: kume@jichi.ac.jp, eternalricenikko98@gmail.com

A putative inhibitory mechanism in the tenase complex responsible for loss of coagulation function in acquired haemophilia A patients with anti-C2 autoantibodies

Tomoko Matsumoto; Keiji Nogami; Kenichi Ogiwara; Midori Shima
Department of Pediatrics, Nara Medical University, Kashihara, Japan

Summary

Acquired haemophilia A (AHA) is caused by the development of factor (F)VIII autoantibodies, demonstrating type 1 or type 2 inhibitory behaviour, and results in more serious haemorrhagic symptoms than in congenital severe HA. The reason(s) for this remains unknown, however. The global coagulation assays, thrombin generation tests and clot waveform analysis, demonstrated that coagulation parameters in patients with AHA-type 2 inhibitor were more significantly depressed than those in patients with moderate HA with similar FVIII activities. Thrombin and intrinsic FXa generation tests were significantly depressed in AHA-type 1 and AHA-type 2 compared to severe HA, and more defective in AHA-type 1 than in AHA-type 2. To investigate these inhibitory mechanism(s), anti-FVIII autoantibodies were purified from AHA plasmas. AHA-type 1 autoantibodies, containing an anti-C2 ESH4-epitope, blocked FVIII(a)-phospholipid binding, whilst AHA-type 2, containing an anti-C2 ESH8-epitope, inhibited thrombin-catalysed FVIII activation. The coagulation function in a reconstituted AHA-model containing exogenous ESH4 or ESH8 was more abnormal than in severe HA. The addition of anti-FIX antibody to FVIII-deficient plasma resulted in lower coagulation function than its absence. These results support the concept that global coagulation might be more suppressed in AHA than in severe HA due to the inhibition of FIXa-dependent FX activation by steric hindrance in the presence of FVIII-anti-C2 autoantibodies. Additionally, AHA-type 1 inhibitors prevented FVIIIa-phospholipid binding, essential for the tenase complex, whilst AHA-type 2 antibodies decreased FXa generation by inhibiting thrombin-catalysed FVIII activation. These two distinct mechanisms might, in part, contribute to and exacerbate the serious haemorrhagic symptoms in AHA.

Keywords

Acquired haemophilia A, anti-C2 autoantibody, thrombin generation, tenase complex, FXa generation

Correspondence to:
Keiji Nogami, MD, PhD
Department of Pediatrics, Nara Medical University
840 Shijo-cho, Kashihara, Nara 634–8522, Japan
Tel.: +81 744 29 8881, Fax: +81 744 24 9222
E-mail: roc-noga@naramed-u.ac.jp

Presented in abstract form at the 52nd annual meeting of the American Society of Hematology, Orlando, Florida, USA, December 6, 2010.

Financial support:
This work was partly supported by the grants for Bayer Hemophilia Award, 2009 and MEXT KAKENHI 21591370, 2009.

Received: May 16, 2011
Accepted after major revision: November 20, 2011
Prepublished online: January 11, 2012
doi:10.1160/TH11-05-0331
Thromb Haemost 2012; 107: ■■■

Introduction

Factor (F)VIII, a protein deficient or defective in individuals with severe congenital bleeding disorder, haemophilia A (HA), functions as a cofactor in the tenase complex, responsible for phospholipid (PL)-dependent conversion of FX to FXa by FIXa (1). FVIII circulates as a complex with von Willebrand factor (VWF) that protects and stabilises the cofactor (2). FVIII is synthesised as a single chain molecule consisting of 2,332 amino acid residues, and is arranged into three domains, A1-A2-B-A3-C1-C2. FVIII is processed into a series of metal ion-dependent heterodimers, generating a heavy chain (HCh) consisting of A1 and A2 domains together with heterogenous fragments of partially proteolysed B domain linked to a light chain (LCh) consisting of A3, C1, and C2 domains (3). The catalytic efficiency of FVIII in the tenase complex is markedly enhanced by conversion into FVIIIa, by limited proteolysis by thrombin (and FXa) (4). Both enzymes proteolyse the HCh at Arg^{372} and Arg^{740}, and produce 50-kDa A1 and 40-kDa A2 subunits. The 80-kDa LCh is cleaved at Arg^{1689} generating a 70-kDa subunit. Proteolysis at Arg^{372} and Arg^{1689} is essential for generating FVIIIa cofactor activity (5). FVIIIa activity is down-regulated by serine proteases including activated protein C, following cleavage at Arg^{336} (4, 6).

FVIII inhibitors develop as alloantibodies (alloAbs) in severe HA patients multi-treated with FVIII concentrates, and also as autoantibodies (autoAbs) in previously normal individuals, particularly in elderly people, patients with autoimmune diseases, pregnant women, and women in the postpartum period. The appearance of autoAbs usually results in severe haemorrhagic symptoms in what is described as acquired HA (AHA). Antibodies of this nature inhibit FVIII activity (FVIII:C) either completely or incompletely at saturating concentrations, corresponding to type 1